

1988

The Tensile Strength of Liquid Helium Four

Joel Alan Nissen
Portland State University

Let us know how access to this document benefits you.

Follow this and additional works at: http://pdxscholar.library.pdx.edu/open_access_etds

Recommended Citation

Nissen, Joel Alan, "The Tensile Strength of Liquid Helium Four" (1988). *Dissertations and Theses*. Paper 1357.

[10.15760/etd.1356](https://pdxscholar.library.pdx.edu/open_access_etds/10.15760/etd.1356)

This Dissertation is brought to you for free and open access. It has been accepted for inclusion in Dissertations and Theses by an authorized administrator of PDXScholar. For more information, please contact pdxscholar@pdx.edu.

THE TENSILE STRENGTH
OF LIQUID HELIUM FOUR

by

JOEL ALAN NISSEN

A dissertation submitted in partial fulfillment of the
requirements for the degree of

DOCTOR OF PHILOSOPHY
in
ENVIRONMENTAL SCIENCES AND RESOURCES/PHYSICS

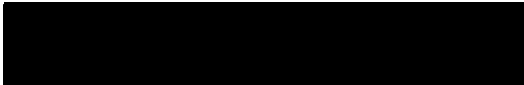
Portland State University

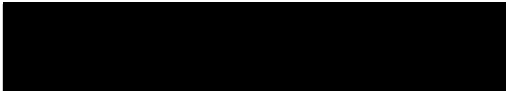
1988


TO THE OFFICE OF GRADUATE STUDIES:

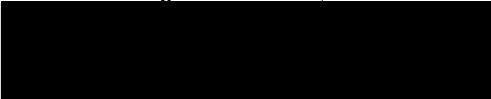
The members of the Committee approve the dissertation
of Joel Alan Nissen presented July 29, 1988.

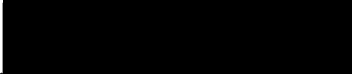

Erik Bodegom, Chair



Laird C. Brodie


Jack S. Semura

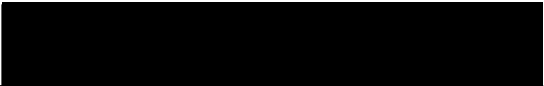

Alan Cresswell


Stanley S. Hillman


Robert O'Brien


Lee W. Casperson

APPROVED:


Pavel K. Smejtek, Director of ESR Program


Bernard Ross, Vice Provost for Graduate Studies

AN ABSTRACT OF THE DISSERTATION OF Joel Alan Nissen for
the Doctor of Philosophy in Environmental Sciences and
Resources/Physics presented July 29, 1988

Title: The Tensile Strength of Liquid Helium Four

APPROVED BY THE MEMBERS OF THE DISSERTATION COMMITTEE:

[REDACTED]

Erik Bodegom, Chair

[REDACTED]

Laird C. Brodie

[REDACTED]

Jack S. Semura

[REDACTED]

Alan Cresswell

[REDACTED]

Stanley S. Hillman

[REDACTED]

Robert O'Brien

[REDACTED]

Lee W. Casperson

It is well known that most liquids exhibit a tensile strength which is much smaller in magnitude than the tensile strength predicted by homogeneous nucleation theory. This lack of agreement is usually attributed to the difficulty of preparing liquid samples free from foreign gases which act as heterogeneous nucleation sites. Liquid helium occupies a unique place among liquids for tensile strength measurements because all foreign gases are frozen out at liquid helium temperatures. Furthermore, superfluid ^4He should fill all crevices on solid surfaces, eliminating the chance of heterogeneous nucleation on helium vapor pockets. Despite the quantum mechanical nature of liquid helium, Becker-Doring theory of nucleation of the vapor phase from the liquid phase should be valid down to 0.3 K in ^4He , yet previous results have been in stark disagreement with the theory.

In this study, a piezoelectric transducer in the form of a hemispherical shell was used to focus high-intensity ultrasound into a small volume of ^4He . The transducer was gated at its resonant frequency of 566 kHz with gate widths of less than 1 msec in order to minimize the effects of transducer heating and acoustic streaming. The onset of nucleation was detected from the absorption of acoustic energy and the scattering of laser light from microscopic bubbles. A new theory for the diffraction of light from the focal zone of a spherical converging sound

wave was developed to confirm calculations of the acoustic pressure amplitude at the focus of the piezoelectric transducer, calculations which were based on the acoustic power radiated into the liquid and the nonlinear absorption of sound.

The experimental results were in agreement with homogeneous nucleation theory for a nucleation rate of approximately 10^{15} critical size bubbles/sec-cm³. This is only the third liquid for which the theoretical tensile strength has been reached and it confirms homogeneous nucleation theory over a range three times greater than any other experiment. A noticeable decrease in the magnitude of the tensile strength was noted at temperatures near the lambda transition and a hypothesis that bubbles are being nucleated heterogeneously on quantized vortices is presented.

ACKNOWLEDGMENTS

This dissertation is dedicated to Lee Stegner for editing the manuscript and for her support and encouragement. I owe a great deal to Dr. Erik Bodegom for his patient help with experiments and lively insightful discussions. His sense of humor made the exhausting work of a series of helium experiments enjoyable. I will always be grateful to Dr. Laird Brodie for starting me on this project with the crucial observation that the previous attempts at reaching the theoretical tensile strength of helium were quasistatic experiments and that in analogy with superheating of liquids, a tensile strength experiment must be done quickly. This was my guiding principle throughout the five years of tensile strength research. I would also like to thank Dr. Jack Semura for his thought provoking questions and his seemingly boundless enthusiasm.

I am also indebted to the invaluable technical assistance of Mr. Garo Arakelian, Mr. Brian McLaughlin, Mr. Lee Thannum and especially Mr. Rudi Zupan. Finally I would like to thank Dr. Alan Cresswell and Mr. Joseph Walters for their friendship.

TABLE OF CONTENTS

	PAGE
ACKNOWLEDGMENTS	iii
LIST OF TABLES	vi
LIST OF FIGURES	vii
 CHAPTER	
I INTRODUCTION	1
II HOMOGENEOUS NUCLEATION THEORY	7
Metastable States	7
The Work Required to Form a Bubble	11
III NUCLEATION AT WEAK SPOTS	17
Nucleation on Trapped Vapor	17
Heterogeneous Nucleation	
on Solid Surfaces	19
Ionizing Radiation	24
Quantized Vortices	25
IV TIME DEVELOPMENT OF NUCLEATION	32
Homogeneous Nucleation	
as a Spontaneous Event	32
Heterogeneous Nucleation	
on Solid Surfaces	35
Nucleation Due to Ionizing Radiation	37

	v
Heterogeneous Nucleation on Vortices . . .	39
Conclusion	40
V TENSILE STRENGTH MEASUREMENTS IN ⁴ HE	42
Introduction	42
Apparatus	43
Measurements	48
Observations	51
Comparison with Theory	52
The Temperature Change	
The Nucleation Rate Far from the	
Lambda Transition	
The Nucleation Rate Near the Lambda	
Transition	
IV SUMMARY AND CONCLUSION	70
REFERENCES	73
APPENDIX A	79
APPENDIX B	88

LIST OF TABLES

TABLE		PAGE
I	The Parameters for Calculating the Heat Capacity as a Function of Pressure and Temperature	55
II	The Parameters for Calculating the Expansivity as a Function of Pressure and Temperature	56
III	The Nonlinearity Parameter B/A	85

LIST OF FIGURES

FIGURE	PAGE
1. At Equilibrium, a van der Waals Substance Exhibits a Phase Change	9
2. A Schematic Representation of the Work Needed to Form a Critical Size Bubble as a Function of Bubble Radius	12
3. The Tensile Strength of Liquid Helium Four According to the Becker-Doring Theory	16
4a. A Bubble Residing on a Flat Smooth Surface	20
4b. For a Deeply Undercut Cavity, Heterogeneous Nucleation Is Possible Even When the Contact Angle is Zero	20
5. If a Liquid Is Slowly Expanded by Means of a Piston with One Heterogeneous Nucleation Site, Then the Bubble Formed at that Site Will Have Ample Time to Grow	38
6. A Schematic of the Optical Arrangement for Detecting Cavitation	45
7. A Schematic of the Electrical Circuit for Powering the Piezoelectric Transducer	46

8.	At $t=0$ Power to the Piezoelectric Transducer is Gated on, 40 Microseconds Later the Sound Reaches the Laser Beam and Light Is Diffracted out of the Central Diffraction Order	19
9.	A Photograph of the Cavitation Zone Exposed within 0.5 msec of the Initiation of Cavitation	53
10.	The Experimentally Obtained Data Agree with the Theoretical Homogeneous Nucleation Rate	50
11.	At Point A Critical Size Bubbles Are Formed . .	62
12.	Near the Extrapolated Lambda Line the Nucleation Rate Decreases	65
13.	The Work Necessary to Form a Critical Size Bubble and the Energy of a Vortex Ring . .	67
14.	Schematic of the Circuit Used to Measure the Impedance of the Piezoelectric transducer	80
15.	The Equivalent Circuit for a Piezoelectric Plate Operated at its Series Resonance . .	80
16.	A Uniform Acoustic Beam with Propagation Vector in the z Direction Diffracts Light Incident from the Left into Discrete Diffraction Orders	90

17. In the Parafocal Region of a Focused Sound Beam, the Initially Spherical Wave Front Flattens Out and Can Be Approximated by Plane Wave-Fronts Traveling in the z Direction 93
18. The Radial Pressure Distribution in the Focal Plane of the Transducer Is Replaced by a Pressure Distribution with a Constant Pressure Amplitude 95
19. Laser Light Is Shaped by a Cylindrical Lens and Brought to a Focus Coinciding with the Acoustic Focal Zone of a Piezoelectric Transducer 99
20. The Zero Order Diffracted Light Intensity in the First 0.8 ms After Power Is Applied to the Piezoelectric Transducer 101
21. The Solid Line Represents the Theoretically Obtained Raman-Nath Parameter as a Function of Pressure 104

CHAPTER I

INTRODUCTION

Phase transitions are ubiquitous in nature: evaporation and condensation of water allow life to exist on land; phase transitions occur in chemical reactions; even the early universe is currently described as a sequence of phase transitions. This thesis addresses a particularly simple phase transition, the homogeneous nucleation from the liquid phase to the vapor phase of pure substances, in particular of helium.

The theory of homogeneous nucleation was first developed by Volmer and Weber in 1926. Since then the various modifications of this theory, such as the Becker-Doring theory, have met with great success in predicting the maximum superheat attainable for liquids. Superheating experiments, however, are limited to the positive pressure region and therefore test nucleation theory only over a narrow range of temperatures and pressures; the greater part of the homogeneous nucleation curve lies in the negative pressure region for most liquids and is only accessible by tensile strength measurements.

Everyday experience shows us that solid material is

able to sustain large tensile stresses. The tensile strength, or in other words the breaking point, of the material will depend upon the strength of intermolecular cohesive forces which must be overcome in order to separate the material. Liquids, like solids, exhibit cohesive forces between molecules and therefore are also able to sustain tensile stress. When the breaking point is reached, vapor bubbles are formed in the liquid.

While for solids the stress must be described by tensors, for liquids we can use the much simpler concept of negative pressure indicating that the applied force is directed outward from the volume of liquid under consideration. Although there is little direct experience with negative pressure in daily life, negative pressure is a common and important occurrence in nature. Tall trees, for example, are able to transport sap to their upper leaves by maintaining up to 25 atmospheres of negative pressure at the top branches (Scholander 1972), and common ferns explosively discharge their spores by developing - 200 atmospheres of negative pressure in water (King 1944).

Despite active research to measure the tensile strength of water over the last 140 years, it is safe to say that the theoretical tensile strength of about -1,400 atmospheres at 20° C has not been reached. The experimentally measured tensile strength varies from as weak as a few tens of atmospheres for acoustic

experiments to several hundred atmospheres for spinning capillaries and Berthelot tubes. The failure to reach the predicted breaking point appears to lie in the difficulty of obtaining pure liquid samples that are free of solid particles and dissolved foreign gases. Solid particles, or motes, are able to reduce the magnitude of the tensile strength by trapping small stable gas pockets in cracks and pits on their surfaces. Even if a particle is perfectly wetted by the liquid, bubble formation may be enhanced by surface irregularities. A process in which the liquid breaks due to a foreign substance is often termed cavitation to distinguish it from the tensile strength, which is a property of the pure liquid.

It is perhaps not surprising that the tensile strength of water has not been reached, since water is notoriously difficult to purify because of its strong solvent properties. In fact the theoretical tensile strength of only three liquids has ever been reached. Apfel (1971) reached the predicted tensile strength for for both n-hexane and ether. Recently at Portland State University, we reached the theoretical tensile strength of a third liquid, helium II (Nissen et al. 1988) and measurements have now been extended to helium I. The tensile strength of helium I and helium II is the subject of this thesis.

Helium is unique among liquids in studying tensile

strength for several reasons. Foremost is that since helium is a liquid only at temperatures colder than 5.2 K, all other gases are frozen out of the helium and are therefore unavailable as gas pockets which act to lower the tensile strength. Stable pockets of helium vapor residing on surfaces are still a possible mechanism for lowering the magnitude of the tensile strength. This mechanism, however, has a low probability of occurring due to the small surface tension of helium (0.35 ergs/cm^2 compared with $20 - 70 \text{ ergs/cm}^2$ for most liquids). A liquid with a low surface tension, like liquid helium, is a very good wetting agent and will fill most of the surface irregularities.

The situation is even more advantageous in liquid helium four at temperatures below 2.17 K, the transition temperature between the helium I and helium II known as the lambda transition. Above the lambda transition, helium I behaves in most respects as any normal fluid. Helium II, however, behaves as if it is a mixture of normal fluid and a superfluid. Many of the properties of the superfluid can be understood from the quantum mechanical laws of a Bose gas. One of the many interesting properties of the superfluid is its ability to flow into minute channels thereby filling any cracks or pits, thus eliminating these as sites for nucleation due to trapped vapor. It is unlikely that helium vapor will

even form when helium II is in equilibrium at its saturation vapor pressure curve since the phenomenon of second sound carries local heat fluctuations away so rapidly that thermal activation of nucleation sites is unlikely. The lack of effervescent boiling on the vapor pressure curve is evidence of this phenomenon.

Finally, since helium remains a liquid even at zero kelvin, there exists the possibility of observing a new and fundamental limit to the tensile strength based not on thermally induced fluctuations, but based on the quantum mechanical uncertainty in the position of the helium atoms.

This research has implications for several practical applications. It seems probable that large-scale uses of superconductors such as energy transport, storage or generation will be developed. In the foreseeable future, these systems will rely upon cryogenic liquids to act as coolants. It should be mentioned here, that with the advent of the high T_c superconductors, cooling to liquid nitrogen temperature (77 K) is sufficient for many superconductor applications. For large-scale use, however, the added cost of cooling to liquid helium temperature (4.2 K) is compensated by the ease of construction and by the increased current density of conventional superconductors. Instrumentation is another field that widely uses liquid helium as a coolant for the

fine sensitivity that can be achieved by reducing thermal noise. Orbiting infrared telescopes and SQUIDs, extremely sensitive devices which measure the earth's magnetic field as well as magnetic fields in the human brain, are examples of devices that require liquid helium temperatures in order to operate. In all of these applications, vapor nucleation, either from transient heating or from depressurization (e.g. bubbles forming in pumping systems), can cause shutdown or destruction of the apparatus.

Besides the practical significance, this research is important for two fundamental reasons. First, a thorough study of the tensile strength of liquid helium over an extended temperature range has resolved the long-standing discrepancies among previous results. Second, a corresponding states analysis, which allows comparison of one liquid to another, reveals that our experimental results have tripled the region over which homogeneous nucleation theory has been tested for any liquid.

CHAPTER II

HOMOGENEOUS NUCLEATION THEORY

METASTABLE STATES

In reality the tensile strength of a liquid is not a single value but is the negative pressure portion of a family of curves. The complete set of curves can be described by homogeneous nucleation theories for liquid to vapor phase transitions of pure substances. These theories, e.g. Becker-Doring, calculate the rate of bubble formation. The theories apply equally to situations in which the liquid is brought into its metastable region by stretching the liquid at constant temperature (tensile strength experiments), by superheating at constant positive pressure, or a combination of the two methods.

The principle of homogeneous nucleation theories can be illustrated by the phase transition occurring in a van der Waals gas. It is useful to write the van der Waals equation in terms of reduced coordinates: P/P_C , T/T_C , and V/V_C . The variables P , T , and V are the pressure, temperature, and volume of the system. The subscripted variables refer to the value of the variable at the critical point.

$$\frac{P}{P_c} = \frac{8T/T_c}{3V/V_c - 1} - \frac{3}{(V/V_c)^2} \quad (2.1)$$

The advantage of writing equations in this manner is that all liquids follow a universal scaling law in reduced coordinates (with suitable modifications for quantum mechanical effects). This facilitates comparison of different liquids.

The van der Waals equation is cubic in V and exhibits the loop shown in Fig. 1 along any isotherm with $T < T_c$. At point A the system is in the stable liquid phase. If the volume is increased slowly and isothermally in such a way that the liquid remains in equilibrium, the pressure of the liquid will monotonically decrease until point B is reached on the liquid saturation curve. By continuing expansion of the system at equilibrium, vapor will be formed and will coexist in stable equilibrium with the liquid. The curve, BF, along which the liquid and vapor coexist, is found by means of the Maxwell construction. The construction is formed by requiring equal areas under the curves BCD and DEF. The molar fraction of liquid to vapor is determined by the position along BF. This curve is a straight line when projected onto the P-V plane. The P-T projection of the binodal takes the shape of a curve terminating at the critical point. In the P-T projection, the binodal is alternately

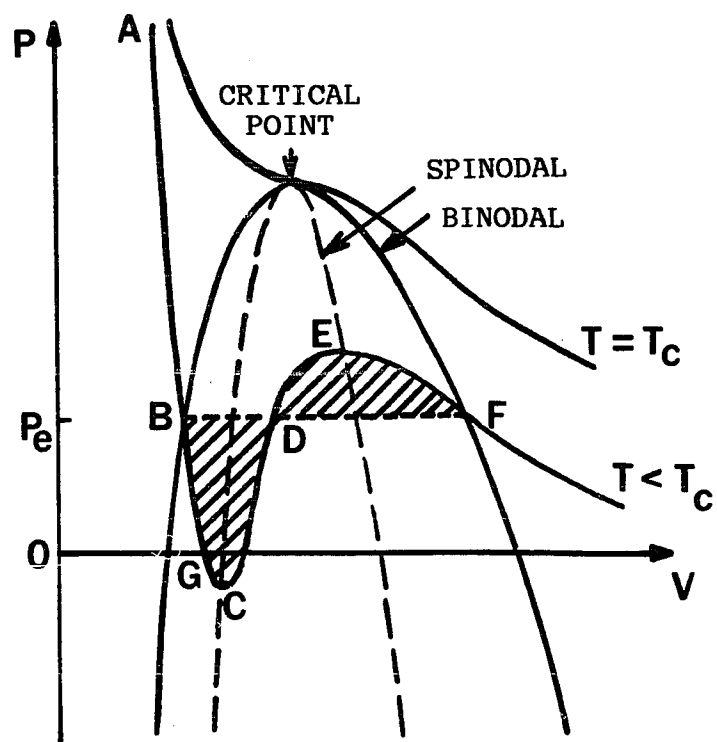


Figure 1. At equilibrium, a van der Waals substance exhibits a phase change along the saturated vapor pressure curve, B-F, for isotherms with T less than the critical temperature. If the volume is rapidly increased from point A, then the van der Waals substance can penetrate into the metastable liquid region along curve B-C. For low temperatures, negative pressures can be reached such as the point G.

referred to as the coexistence curve, or the saturated vapor pressure curve. At point F the vapor saturation curve is reached and the system consists entirely of vapor. Further expansion does not lead to other phase transitions in a van der Waals substance.

If instead of expanding the stable liquid slowly at equilibrium, the volume is suddenly increased, the liquid will penetrate into the metastable region along the curve BC. The metastable state is a state in which the Gibbs free energy is at a local rather than a global minimum. After a characteristic mean time, $\langle \tau \rangle$, which is highly dependent on the depth of penetration into the metastable region, the liquid will decompose to a stable equilibrium configuration on the coexistence curve. When T/T_c is less than about 0.8, rapid stretching of the liquid into the metastable region can result in negative pressure such as point G in Fig. 1. Point C lies on the liquid spinodal, the curve marking the transition to instability, and represents a true limit to the tensile strength of the liquid. In practice this limit is not reached, rather the tensile strength is determined by kinetic rates of bubble formation in the metastable region.

THE WORK REQUIRED TO FORM A BUBBLE

The rate of bubble formation is calculated by considering the minimum work that must be done to form a vapor bubble in the liquid. An amount of work equal to the surface tension times the surface area, σA , must be done to form a cavity. Part of the work is done by the gas vaporized into the cavity so that the total work (W) needed to form a bubble is

$$W = \sigma A - (P_G - P_L)V_G + x(\mu_G - \mu_L) \quad (2.2)$$

where P_G is the pressure of the gas in the bubble, P_L is the pressure of the surrounding liquid, V_G is the volume of the bubble, x is the number of molecules vaporized into the cavity, μ_G and μ_L are the chemical potentials of the gas and vapor respectively. On the coexistence curve, the pressure of the gas and the pressure of the liquid are equal to the vapor pressure. The chemical potentials are also equal on the coexistence curve, so that the work necessary to form a bubble rises to infinity as the bubble radius is increased (curve a of Fig.2). If the liquid is brought rapidly into the metastable region by means of a pressure excursion then the following conditions will hold: $P_L < P_G$ and $\mu_G < \mu_L$. Under these conditions, the work necessary to form a bubble increases to a maximum

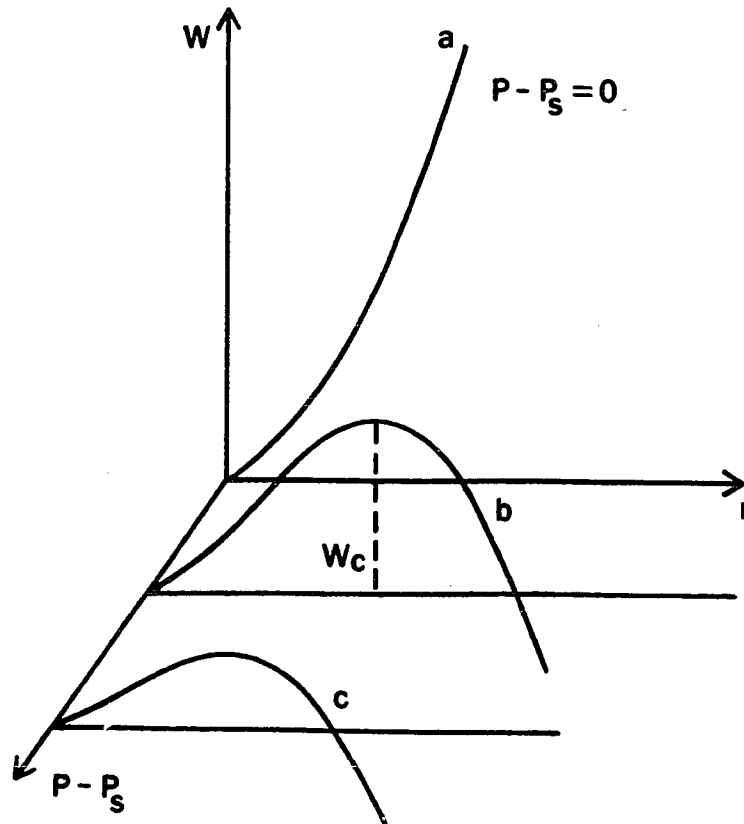


Figure 2. A schematic representation of the work needed to form a critical size bubble as a function of bubble radius. On the saturated vapor pressure curve, the work rises monotonically (curve a). As the liquid is brought into the metastable region, the work necessary to form a bubble of radius r first increases, reaches a maximum at the critical radius, and then monotonically decreases (curve b). Curve c shows the lower barrier height and smaller critical radius for a liquid far from the saturated vapor pressure curve.

then decreases, eventually becoming negative as the bubble radius is increased (curve b of Fig. 2). The work function is essentially a barrier to the formation of bubbles by random thermal fluctuations. If random fluctuations produce a cavity with a radius smaller than r_c , the radius corresponding to the peak in the work function, the bubble will spontaneously collapse. The vast majority of the random fluctuations will result in bubbles too small to be viable. If, on the other hand, the random fluctuations lead to the formation of a bubble with a radius larger than r_c , the bubble can only decrease its energy by growing. The further the excursion into the metastable region, the lower the height of the barrier (curve c of Fig. 2). Therefore, the probability that a bubble will be formed with a radius greater than r_c will be greatly increased.

The location of the peak of the work function for a bubble in chemical and mechanical equilibrium is obtained by differentiation and is found at the critical radius, r_c , given by

$$P_G = P_L + \frac{2\sigma}{r_c} \quad (2.3)$$

Bubbles with radii smaller than r_c are unstable and so tend to collapse, while bubbles with radii larger than r_c

will spontaneously grow as long as the liquid pressure and temperature are held constant. Liquid helium has a critical radius of less than 2 nm over most of its temperature range.

The work (W_C) required to form a critical size bubble can be used to calculate J , the rate of formation of bubbles per unit volume in steady state. J can be calculated based upon heterophase fluctuation theory

$$J \propto \exp(-W_C/kT) \quad (2.4)$$

k being Boltzman's constant and T being the temperature.

Blander and Katz (1975) write the rate equation as

$$J = N \left[\frac{2\sigma}{\pi mB} \right]^{3/2} \exp \left[\frac{-16\pi\sigma^3}{3kT (P_V - P_L)^2} \right] \quad (2.5)$$

where N is the number density of the liquid, m is the molecular mass, and B is a factor which is approximately 1 for cavitation and 2/3 for superheating. In the laboratory the equilibrium vapor pressure, P_e , is the quantity that is directly measured, rather than P_V , the vapor pressure inside the bubble. Therefore it is convenient to introduce the Poynting correction, δ , relating P_e to P_V

$$P_V - P_L \cong (P_e - P_L)^\delta \quad (2.6)$$

The Poynting correction can be approximated from the equilibrium values of ρ_G and ρ_L , the density of the gas and liquid respectively, in the following way

$$\delta \cong 1 - \left(\frac{\rho_G}{\rho_L} \right) + \frac{1}{2} \left(\frac{\rho_G}{\rho_L} \right)^2 \quad (2.7)$$

Figure 3 displays three curves for homogeneous nucleation of ^4He . We will primarily be concerned in this paper with the negative pressure region of the nucleation curve. One notable feature of this graph is that even a small pressure or temperature change makes an enormous change in the nucleation rate. Above 4 K the rate of bubble formation per cm^3 varies from $J = 10^{-15}$ bubbles/sec (one bubble every 30 million years on the average) to $J = 10^{15}$ bubbles formed every second, within a pressure change of a few tenths of an atmosphere. The other notable feature is that at temperatures below 0.5 K the nucleation theories so far discussed are no longer sufficient to describe the fluctuations. At these low temperatures Akulichev (1975) predicts that quantum mechanical fluctuations will predominate over thermal fluctuations and the nucleation rate will become temperature independent. This phenomenon, which has never been observed, is termed quantum nucleation.

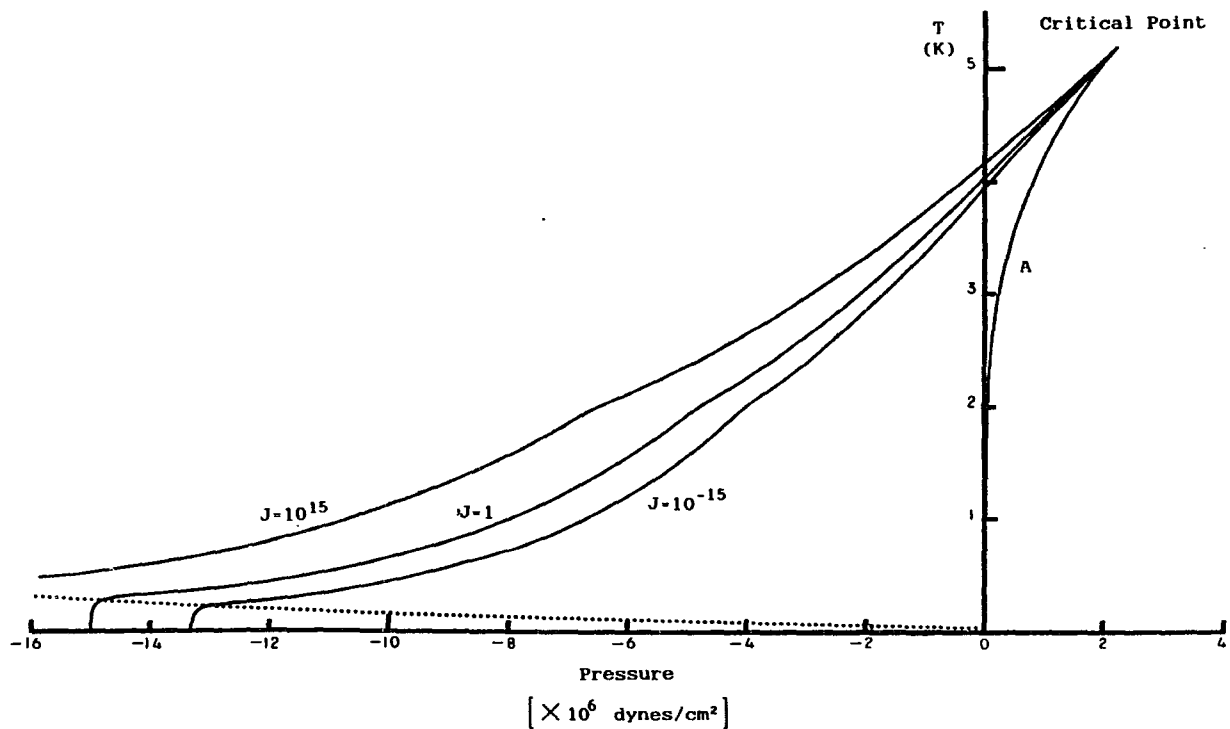


Figure 3. The tensile strength of liquid helium four according to the Becker-Doring theory for three values of the formation of critical nuclei per second per cubic centimeter. The curve A is the equilibrium vapor pressure curve and the dotted line is the limit of quantum nucleation.

CHAPTER III

NUCLEATION AT WEAK SPOTS

NUCLEATION ON TRAPPED VAPOR

Most liquids exhibit cavitation thresholds which are much smaller than their predicted tensile strength. As was stated in the introduction, this is thought to be due to stable pockets of undissolved gas or vapor residing in narrow pits on solid surfaces. Even if the experiment is conducted far from any container walls, there will likely be microscopic solid inclusions (motes) which trap foreign gas and helium vapor. Because of the low temperature at which ^4He liquefies, there can be no foreign gas except possibly minute quantities of ^3He which can reside on motes. Additionally, because of helium's low density and low viscosity, motes will drop to the bottom of the dewar. Furthermore, due to the ability of the superfluid film to penetrate fine pores, displacing any trapped vapor, helium II should be the ideal liquid for tensile strength measurements. The excellent wetting property of superfluid helium can be extended to helium I by first filling the crevices in solid surfaces with the superfluid and then allowing the helium to warm to helium I

temperatures.

The ability of superfluid to fill minute surface irregularities motivated Beams (1956) to conduct a variety of experiments attempting to measure the tensile strength of helium. His reported value of the tensile strength was -0.16 bar at 1.8 K. (1 atmosphere ≈ 1 bar $\equiv 10^6$ dynes/cm²) This was in rough agreement with an earlier measurement by Misener and Herbert (1956), which gave a result of -0.3 bar for helium II. Since then, over twenty reports relating to the tensile strength of helium II have appeared in the scientific literature trying to resolve the stark discrepancy between the predicted tensile strength of -4 to -12 bars and the experimental values. In several of these experiments bubbles were observed to originate preferentially on surfaces, which may indicate that a few vapor pockets remain on the solid surfaces for a significant time. Sinha (1980) found in superheating experiments in helium I that, once formed, subcritical size bubbles can reside on surface irregularities for up to several seconds. Under these conditions the vapor inside the bubble is in a supercooled metastable state. Still, a lifetime of a few seconds cannot account for the low value of the tensile strength observed in the large variety of experimental techniques that have been employed. Other mechanisms of nucleation must be examined.

HETEROGENEOUS NUCLEATION ON SOLID SURFACES

Any mechanism that locally enhances the probability of a vapor nucleus being spontaneously formed by a process other than homogeneous nucleation is called heterogeneous nucleation. When a solid surface is present in the liquid, there will be crevices on the solid surface which may act as weak sites for nucleation even when no vapor is initially present. Whether these sites reduce the measured magnitude of the tensile strength or not depends upon three factors: the ratio of molecules of liquid on the solid surface to the number of molecules in the bulk liquid, the microgeometry of the surface, and θ , the contact angle (Fig. 4a).

The contact angle is determined by the relative magnitudes of the surface tension at three different interfaces: the liquid-vapor interface, σ , the solid-liquid interface, σ_{sl} , and the solid-vapor interface, σ_{sv} . The contact angle, θ , is then given by the relation

$$\cos\theta = (\sigma_{sv} - \sigma_{sl})/\sigma \quad (3.1)$$

subject to the restriction

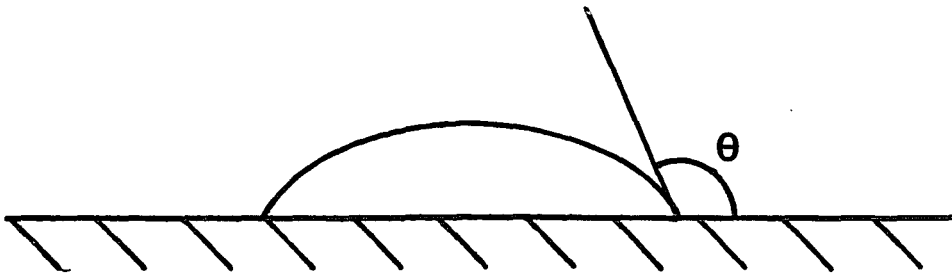


Figure 4a. A bubble with contact angle θ relative to a flat smooth surface.

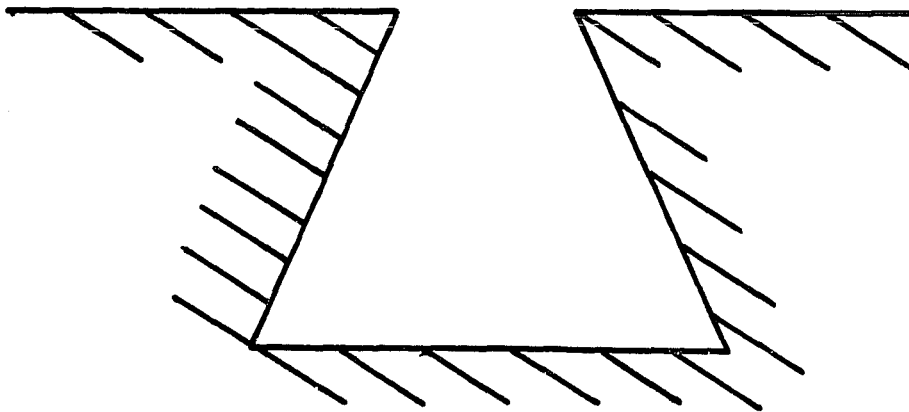


Figure 4b. For a deeply undercut cavity, heterogeneous nucleation is possible even when the contact angle is zero.

$$\sigma_{sv} - \sigma_{sl} \leq \sigma \quad (3.2)$$

to ensure that $\cos\theta \leq 1$. The contact angle for liquid helium is expected to be zero for all solids, i.e. perfect wetting of the surface (Good and Ferry 1962).

The rate equation for nucleation of vapor cavities is related to W_c , the work necessary to form a bubble through homogeneous nucleation, by the following expression

$$J_{het} = N^{2/3} \cdot c_2 \frac{\rho_L}{\rho_V} \left[\frac{2\sigma}{n m B F} \right]^{1/2} \exp\left[\frac{-W_c \cdot F}{kT} \right] \quad (3.3)$$

where J_{het} is the nucleation rate per unit surface area and F is the work required to form a bubble at the surface divided by the work required to form a critical size bubble in the homogeneous liquid.

$$F \equiv \frac{W_{het}}{W_c} = 3(c_2 + c_3 \cdot \cos\theta) - 2c_1 \quad (3.4)$$

where c_1 , c_2 and c_3 depend on the microgeometry of the solid surface.

Several aspects of Eq. 3.3 can be pointed out in relation to Eq. 2.5, the corresponding rate equation for homogeneous nucleation. The heterogeneous nucleation rate is proportional to $N^{2/3}$ rather than to N for the

homogeneous case, since only the liquid molecules at the solid surface are potential sites for heterogeneous nucleation. Because N is on the order of 10^{22} molecules/cm³, the prefactor for the heterogeneous nucleation rate per unit area is 10^7 times smaller than the prefactor for the homogeneous nucleation rate per unit volume.

The reason that heterogeneous nucleation usually dominates homogeneous nucleation is found in the argument of the exponential term. The effect of heterogeneous nucleation is illustrated by the simplified geometry of a bubble forming on an ideal flat surface (Fig.4a). For $F < 1$, the exponential term for heterogeneous nucleation is greater than the exponential term for homogeneous nucleation. Assuming one square centimeter of solid surface for every cubic centimeter of liquid, Blander and Katz (1975) calculate heterogeneous nucleation dominates only for $F < 0.77$ (contact angles greater than 68°). Thus a perfectly flat, perfectly smooth surface will not cause heterogeneous nucleation in liquid helium.

The surface of a real solid is of course not flat, rather it is covered with pits, crevices and protrusions. These surface irregularities have a considerable influence on the geometric factor, each site having a different value of F . For deeply undercut pits (Fig. 4b), it is possible for F to be less than unity even if the contact

angle is zero (Thormahlen 1987). Heterogeneous nucleation sites with values of $F \ll 1$ will be activated in metastable states close to the saturation curve. As the liquid is brought further into the metastable region, more and more sites, with increasing values of F , will make significant contributions to the nucleation rate.

The rate expression for nucleation on a surface with a variety of surface features must take into account the relative number of heterogeneous nucleation sites corresponding to each F_i . J_{het} becomes the sum of the nucleation rate at each site, weighted by n_i , the fraction of the surface covered by that site.

$$J_{\text{het}} = \sum_i n_i S_i \exp\left[\frac{-W_c \cdot F_i}{kT}\right] \quad (3.5)$$

where S_i is the prefactor of Eq. 3.3 for the i th potential nucleation site. In the case of heterogeneous nucleation, the nucleation rate is a complicated function of the precise geometry of the features, the number density of sites, and the degree of metastability of the liquid.

Generally the surface microgeometry is not well enough known to make a calculation of the heterogeneous nucleation rate. However, it is obvious that the likelihood of observing homogeneous nucleation is greatly enhanced under the conditions

$$J_{\text{hom}} \cdot V \gg J_{\text{het}} \cdot S \quad (3.6)$$

where V is the volume of the bulk liquid and S is the surface area of solids in or enclosing volume V . The conditions for attaining homogeneous nucleation in the presence of solids will be examined more closely later in this chapter, in the discussion on the time development of nucleation.

IONIZING RADIATION

Another important mechanism for heterogeneous nucleation of liquids in general and of liquid helium in particular, is the passage of ionizing radiation through the fluid. This is the well-known phenomenon utilized in bubble chambers to visualize the tracks of charged particles. The mechanism by which the bubbles are formed appears to be heat spikes generated by the exchange of energy between the liquid and the secondary electrons scattered from the high-energy incident radiation. The secondary electrons are stopped in the liquid in a distance on the order of 10^{-6} cm, releasing their kinetic energy within 10^{-11} sec, thus locally superheating the liquid to initiate a bubble. Normally the bubble would simply collapse in 10^{-7} sec as the localized heat diffuses outward, but if the liquid is in the metastable state the bubble can continue to grow to visible size. Heat spikes

from the passage of ionizing radiation are thought to be much less effective in producing bubble nucleation in helium II due to the presence of second sound, which rapidly carries away the heat. Attempts by Edwards (1966) to produce bubble trails were unsuccessful, although the same apparatus readily produced visible trails in helium I.

Free electrons have an additional role in heterogeneous nucleation of liquid helium. Due to the Pauli exclusion principle, the electron-helium potential will become repulsive at short range. The potential barrier caused by this repulsive force is approximately 1 eV. It is therefore energetically favorable for the electron to form a spherical cavity in the helium. The radius of the cavity is approximately 1.2 nm, which is commensurate with the radius of a critical size bubble. Bubbles formed in this manner are termed electron bubbles. Akulichev (1986) estimates that the electron bubbles are capable of lowering the magnitude of the cavitation strength of helium to less than half the value predicted by homogeneous nucleation theory.

QUANTIZED VORTICES

Alpha particles are also thought to reduce the tensile strength of helium II, although by a more indirect method than the presence of electron bubbles. As the ion

moves through the helium, it experiences viscous drag forces. Vortex rings are shed from alpha particles with drift velocities greater than about 25 m/sec. Vortices in superfluid helium are quantum mechanical entities, each having quantized angular momentum ℓh . The circulation, κ , is given by

$$\kappa \equiv \oint \mathbf{ds} \cdot \mathbf{v} = \frac{\ell h}{m} \quad (3.7)$$

where ℓ is an integer, m is the mass of a helium atom, and \mathbf{v} is the velocity vector. These quantized vortices can be stable for as long as several hours. Although the mechanism for bubble formation remains obscure, some insight can be gained by considering the total energy, E , of a vortex ring

$$E \approx \frac{1}{2} \rho \kappa^2 r \left[\ln\left(\frac{8r}{a_0}\right) - \frac{7}{4} \right] \quad (3.8)$$

where r is the radius of the ring and $a_0 \sim 0.12$ nm is its core radius. Assuming $\ell = 1$ and a ring of $r = 2$ nm (the radius of a critical size bubble), an energy of 10^{-14} ergs is obtained. This is the same order of magnitude as the work necessary to form a critical size bubble. If the energy from the vortex is somehow converted into work of bubble formation, the bubble will be able to grow to

detectable dimensions if the surrounding liquid is in the metastable region.

Fortunately, ionizing radiation occurs at low levels in nature. In order to minimize the effect of natural radiation on tensile strength experiments, it is only necessary to perform the experiment in a small but nevertheless macroscopic volume and to perform it in a time short enough that the passage of ionizing radiation through the volume is unlikely. The time dependence of heterogeneous nucleation will be examined more closely in the next section.

Vortices are also generated in helium II whenever there is a heat flux above a critical value. To understand this phenomenon two properties of superfluid helium must be presented. First, the superfluid component of helium II carries no entropy. Therefore, if a temperature gradient exists in helium II, it is energetically favorable for the superfluid component to move in the direction of increasing temperature. The fountain effect and second sound (entropy waves which propagate like sound waves) are examples of this property. In order that the density of the fluid remains constant, the normal fluid component moves in the opposite direction to the superfluid component, setting up a counterflow. If the counterflow exceeds a critical value, then vortices are formed through mutual friction. The counterflow is the

macroscopically averaged difference between the normal fluid velocity, v_n , and the superfluid velocity, v_s : $v_{ns} = v_n - v_s$. If the heat flux is large enough, a tangle of vortices is generated which is the equivalent of turbulence in a Newtonian fluid. Ideally there is no need for sources of heat in a tensile strength experiment, but as will be shown later, there are often large heat fluxes due to internal energy losses in ultrasonic transducers.

Another mechanism for the generation of vortices in fluids needs to be considered for spinning capillaries and acoustically induced negative pressure. When angular momentum is imparted to the normal component of helium II, vortex lines are created in the superfluid component. This will inevitably result in vortices being produced in a spinning capillary. In a steady state acoustic experiment there will be mass flow (acoustic streaming) of the liquid caused by radiation pressure. Acoustic streaming is always rotational in nature and so it can result in the formation of vortices. The vortices may be confined to viscous boundary layers near solids where their dimensions are smaller than an acoustic wavelength, or they may exist outside the boundary layer as in Rayleigh streaming where the vortex dimension is on the order of a wavelength.

Smith et.al. (1982) have observed the production of vortices in acoustic fields with pressure amplitudes as

low as 5×10^{-4} bar. They convincingly demonstrated that the white noise in helium II, mistakenly identified as acoustic cavitation by several observers (Finch 1964, 1966a, 1966b, 1967, Mosse 1970, McConnell 1970, Jarman 1970, Shadley 1971, Neppiras 1971, Dhingra 1976) is associated with vortex production in acoustic fields. Although forced bubble oscillations are known to generate subharmonics of the driving frequency, Smith showed that the threshold of subharmonic production as a function of temperature is inconsistent with bubble oscillations. Furthermore, several observers found no effect on the threshold of the cavitation-like noise when the helium bath was overpressurized by as much as 1.5 bars (Finch 1966a, 1966b, Jarman 1970). In some cases the liquid helium did not even momentarily reach the saturation curve, much less negative pressures; therefore, it is hard to see how critical size bubbles could be formed. On the other hand, at driving voltages a magnitude above the noise, they observed that the threshold for visible cavitation increased linearly with overpressure, as would be expected for acoustic cavitation.

It should be emphasized that visible cavitation on superfluid vortices has never been conclusively demonstrated. The one experiment (Edwards 1966) in which visible cavitation was nucleated on vortices was somewhat ambiguous. In this experiment, liquid helium was forced

through three holes of varying sizes, generating vortices. Upon subsequently expanding the volume of the liquid by means of a piston, the helium cavitated more readily than it would have if the vortices were not present. The same researchers found that rotating the expansion chamber at speeds high enough to create 1000-2000 vortex lines had no effect on cavitation. Possibly only vortex rings are effective bubble nucleation sites since they concentrate the vortex energy in a smaller volume. It is premature to rule out quantized vortices as heterogeneous nucleation sites and production of vortices should be avoided. Large heat fluxes as well as high amplitude second sound should be excluded from the volume of interest. In order to avoid heterogeneous nucleation on vortices due to acoustic streaming at viscous boundary layers, solid surfaces should be minimized.

In concluding this section, it is probably safe to say that even though liquid helium is in many respects the ideal liquid for tensile strength measurements, not all the sources of heterogeneous nucleation can be eliminated. The number of heterogeneous nucleation sites can, however, be reduced by optimizing the geometry of the experiment. The ideal tensile strength experiment in helium would be conducted in a small volume away from surfaces and sources of heat or second sound.

CHAPTER IV

TIME DEVELOPMENT OF NUCLEATION

HOMOGENEOUS NUCLEATION AS A SPONTANEOUS EVENT

In the discussion so far, it has been implicit that the rates of homogeneous and heterogeneous nucleation are time independent. This is of course not the case, since the stress on the liquid begins at a definite time, before which the nucleation rate is zero. Furthermore, once the steady state nucleation is reached, the local conditions of pressure, temperature, and available nucleation sites may be drastically altered by the presence of the growing bubbles. It will be shown in this section that this time dependence can be used to increase the probability of observing homogeneous nucleation.

The mean time of expectation of a bubble forming spontaneously with a radius greater than the critical radius can be easily calculated from the rate equation. The expectation time, $\langle \tau \rangle$, is simply

$$\langle \tau \rangle = [V \cdot J(P, T)]^{-1} \quad (4.1)$$

Close to the coexistence curve the barrier height is high

so that the expectation time for a viable nucleus is very long. Therefore, if the pressure (or temperature) is changed rapidly, the liquid can traverse states close to the coexistence curve before a spontaneous nucleation event is likely to occur. As the system penetrates further into the metastable region, the barrier height is decreased, making spontaneous fluctuations with radii greater than r_c more likely. As a result, the expectation time rapidly decreases. Eventually a nucleation rate is reached at which the probability of producing a viable bubble is high. The final state will be determined by the transition time, τ_m , and is given by the inequality

$$\int_0^{\tau_m} V \cdot J(P(t), T(t)) dt \ll 1 \quad (4.2)$$

In other words, the transition into metastability must pass each thermodynamic state of $P + \Delta P$, $T + \Delta T$ in a time interval, Δt , which is much shorter than the expectation time for a viable nucleus to form. In order to penetrate deep into the metastable region, it is necessary to rapidly change the thermodynamic state variables such as the pressure. Note also that for a small volume, the transition time is increased.

Eq. 2.5 assumes that steady state conditions have been reached. The approach to steady state nucleation

takes the form (Abraham 1974)

$$J(t) = J[1 - \exp(-t/\tau_s)] \quad (4.3)$$

where τ_s is the time delay to steady state . This sets the upper limit to the speed at which the experiment can be conducted. Evidently the inequality $\tau_m \gg \tau_s$ must hold in order that an experiment can be compared with theory. The time lag estimated by Sinha (1980) for the liquid to vapor transition over a wide range of helium bath temperatures is from 2 to 10 ns. Any experiment testing homogeneous nucleation theory must last 10 ns or longer following transition to the final metastable state to be considered a steady state experiment.

Once the condition of steady state nucleation is reached, it can only be maintained if the bubbles larger than critical size are removed from the system as fast as they are produced. If the nucleation rate is low, for example several bubbles/cm³-sec, then it is possible to remove them from the volume under stress fast enough for steady state nucleation to be maintained. When penetrating deep into the metastable region, however, the number of bubbles formed is so large that vapor is formed explosively, steady state conditions cannot be maintained, and the liquid-vapor system is removed from deep in the metastable region to a state closer to the coexistence

curve. Decomposition begins when enough vapor is created to limit the transport of energy into the volume of metastable liquid. If energy is not constantly added to the liquid, the system will return to the saturated vapor pressure curve. The time for the system to decompose is characterized by a time constant, τ_d . The magnitude of τ_d will be determined by two factors, the rate of bubble growth and the initial magnitude of steady state nucleation, $J(P,T)$.

The rate of bubble growth is dependent upon the rate of diffusion of vapor into the cavity relative to the rate of condensation on the bubble wall and to the magnitude of viscous forces. Removal of the system from deep in the metastable state is highly dependent on the initial nucleation rate in addition to the growth rate. This is best seen from a phenomenological description of the process that leads to decomposition. In the case of homogeneous nucleation, no error will be introduced by assuming the number of potential nucleation sites is independent of the number of critical size bubbles formed. Initially the critical size bubbles are well separated spatially in the volume of liquid subject to mechanical stress (or increased temperature in the case of a superheated liquid). At this early time the bubbles have little effect on the thermodynamic state variables P and T . The liquid will relax towards the saturated vapor

pressure curve only when the bubbles have grown large enough to effect the pressure or temperature throughout the volume. If the nucleation rate $J(P,T)$ is very low, this process may require one bubble to fill nearly the entire volume under stress before that volume returns to the saturation curve. Since the bubble can only grow at a finite rate, this process takes a relatively long time. If, on the other hand, the nucleation rate is high, the volume will be quickly filled by a myriad of microscopic bubbles and the system will be rapidly removed from deep in the metastable state.

HETEROGENEOUS NUCLEATION ON SOLID SURFACES

Nucleation at solid surfaces is expected to reach the steady state value according to the same laws as homogeneous nucleation. This implies that if an experiment is to be designed to verify steady state homogeneous nucleation theory, then at the time the measurement is made the heterogeneous nucleation at solid interfaces is also in steady state nucleation. Therefore, the time delay associated with the onset of steady state heterogeneous nucleation at a surface cannot be used to eliminate the effects of the solid. Of course if the number of potential homogeneous nucleation sites is vastly greater than the number of heterogeneous nucleation sites, the expectation time for homogeneous nucleation, $\langle \tau \rangle$, will

still be shorter than the expectation time for heterogeneous nucleation. Under these conditions the first viable nuclei are likely to be created in the homogeneous liquid. Furthermore, the rate of bubble formation due to heterogeneous nucleation will be insignificant in comparison to the rate of homogeneous nucleation (Eq. 3.6).

For very rapid excursions, the liquid can be brought far into the metastable region despite the presence of a significant contribution of steady state heterogeneous nucleation. The excursion must be rapid to insure that a thermodynamic state deep in the metastable region is reached before bubble growth at heterogeneous nucleation sites has time to appreciably alter the flow of energy into the liquid.

In order to clarify this point, imagine a perfectly smooth cylinder closed at one end and filled with a liquid which will not cavitate on the cylinder wall. The other end of the cylinder is closed by a piston with one heterogeneous nucleation site (Fig. 5) which has a very high probability of forming a critical size bubble while the liquid is still close to the saturation curve. The piston is slowly pulled out to a point where the probability is essentially one that a bubble is formed at the piston surface and the probability is essentially zero that a bubble is formed in the bulk liquid. In a short

period the bubble will grow and vapor will cover the surface of the piston. The piston can no longer apply stress to the liquid, and the system will return to the equilibrium vapor pressure curve without having reached the predicted tensile strength.

Now the piston is instead pulled rapidly out and the bubble is still formed on the surface. The liquid can still penetrate deeper into the metastable region as long as the bubble on the piston only covers an infinitesimal fraction of the piston surface. If the piston is pulled quickly enough, a very high rate of homogeneous nucleation can be reached, and the single heterogeneous nucleus will add a statistically insignificant error to the nucleation rate.

NUCLEATION DUE TO IONIZING RADIATION

It was stated earlier that the effects of ionizing radiation can be neglected if the volume of metastable liquid is small and the experiment is conducted in a short time. Mate and McCloud (1968) found that the waiting time for rupture of metastable helium II due to ionizing radiation in a 1 cm^3 cell was on the order of 300 sec. This time must be viewed with caution, however, since the experiment was conducted near the saturation curve. Here, initiated bubbles are less likely to reach critical size and therefore tend to collapse before they are detected.

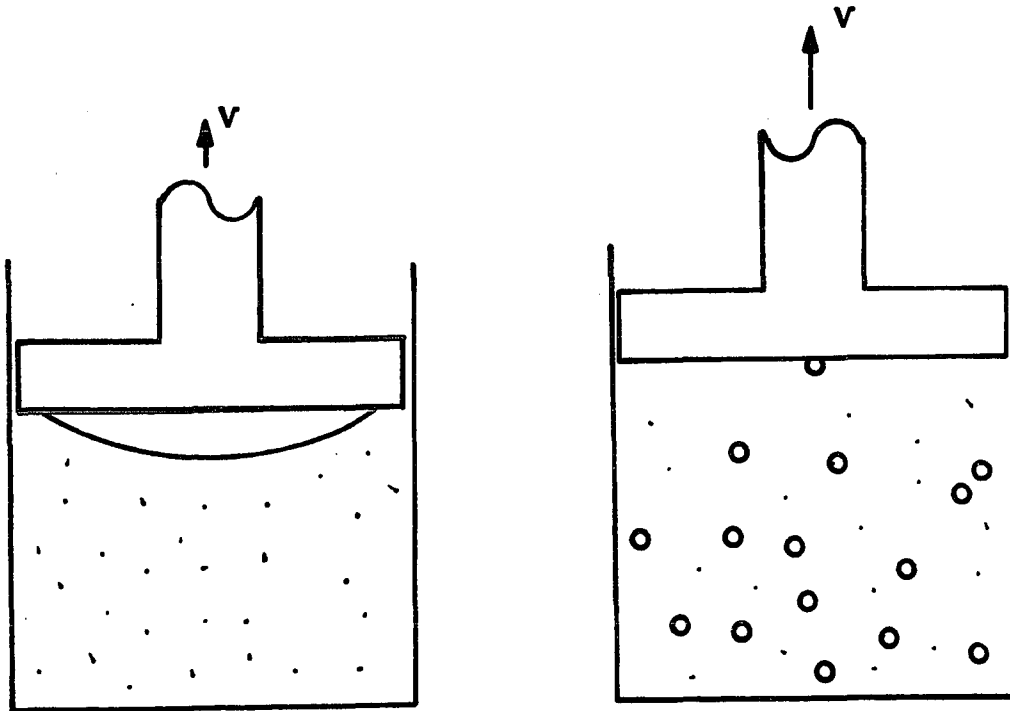


Figure 5. If a liquid is slowly expanded by means of a piston with one heterogeneous nucleation site on its surface, then the bubble formed at that site will have ample time to grow before the liquid can be brought deep into the metastable region. If the volume of the liquid is rapidly increased, then the bubble formed at the heterogeneous nucleation site does not grow large enough to decouple the piston from the liquid before homogeneous nucleation takes place in the bulk liquid.

Skripov et al. (1974) used a capillary filled with highly superheated liquid to study the mean time of expectation for natural radiation to nucleate metastable liquids. They found that in a volume of $3 \times 10^{-2} \text{ cm}^3$ the mean lifetime of metastable n-pentane, n-hexane, diethyl ether, benzene, and hexafluorobenzene was on the order of 10 sec. Using the expectation time found by Skripov as indicative of the sensitivity of metastable liquids to ionizing radiation, it is clear that in a nucleation experiment confined to a reasonably small volume, the effects of ionizing radiation can be neglected when the experiment is conducted within a few milliseconds.

HETEROGENEOUS NUCLEATION ON VORTICES

A similar analysis applies to the matter of heterogeneous nucleation on quantized vortices. In this case the important time scale to consider is the time required to generate the vortices. Vinen (1957) examined the attenuation of second sound in the presence of a steady heat current. The generation of vortex rings was detected by a sudden decrease in the amplitude of the received second sound signal. A time delay was observed between switching on the heat current and the generation of vortex tangles. At heat currents of 0.03 W/cm^2 the time delay was 8.0 sec. As the magnitude of the heat current increased, the time delay decreased, but heat

currents as high as 0.3 W/cm^2 only reduced the time delay to 0.2 sec. This time delay phenomenon is familiar from the classical fluid dynamic behavior of the onset of turbulence.

A caveat must be added to the discussion of creating heterogeneous nucleation sites on vortices. Once formed, vortices can persist in a metastable state for hours after the normal fluid has come to rest, and it has long been suspected that pinned vortices are always present in the superfluid. However, as long as the number density of vortices is kept small, the chances of the vortex effecting the tensile strength measurement can be minimized through use of small volumes.

CONCLUSION

The idea that the zero contact angle and superfluid properties of helium would be sufficient to eliminate heterogeneous nucleation on solid surfaces must be suspect in view of experimental evidence and recent theoretical investigation of nucleation rates in the presence of deeply undercut surface irregularities. Furthermore, ionizing radiation and quantized vortices present serious impediments to observing the tensile strength of helium. In order to optimize the chance of observing homogeneous nucleation, the tensile strength experiment should be conducted in a small volume away from solid surfaces.

It is impossible to eliminate all sources of heterogeneous nucleation and so the tensile strength experiment must quickly reach deep into the metastable region where the resulting high rate of homogeneous nucleation will mask any contribution of heterogeneous nucleation. Under the conditions of intense nucleation rates, the liquid can be expected to rapidly decompose to a liquid-vapor system close to the equilibrium vapor pressure curve. It is this rapid decomposition, not formation of a few macroscopic bubbles, that characterizes the tensile strength.

CHAPTER V

TENSILE STRENGTH MEASUREMENTS IN ^4He

INTRODUCTION

Many of the desirable features of the ideal tensile strength experiment which were presented in the last chapter can be achieved through the use of high-intensity focused ultrasound. One advantage of focused ultrasound is that a high-frequency sound wave can be focused to a very small volume. A volume limited only by diffraction to a focal zone with a radius of one half the acoustic wavelength. Another advantage is that the focal zone is in the bulk liquid, far from any container walls so that the only solid surfaces available for heterogeneous nucleation are motes of frozen air. A third advantage of high-frequency ultrasound is that the excursion into the metastable region can be very rapid. The time required to change the pressure from the saturated vapor pressure curve to the final negative pressure is one quarter the acoustic period. However, acoustic methods are not perfect, their major drawback being the creation of vortices, either from acoustic streaming or from heating of the transducer.

APPARATUS

Short bursts of ultrasound were focused in liquid helium II by a piezoelectric transducer formed in the shape of a hemispherical shell. The transducer, Channel 5400 Navy I, had an inside radius of 0.625 cm and an outside radius of 1.043 cm. It was operated in its thickness mode at the half-wave resonant frequency of 566 kHz. The transducer was held in one of two different configurations depending on whether the experiment was to be conducted in helium I or helium II. The piezoelectric transducer was mounted with the concave side facing down for the helium II experiments. This arrangement was possible because the superfluid properties of helium II prevent vapor from collecting in the inverted cup of the transducer. Three thin wires supported the transducer along its rim at nodal surfaces to minimize ultrasonic radiation into the supports and to minimize distortion of the transducer. Experiments in helium I were conducted with the concave side of the transducer facing up in order to prevent vapor bubbles from collecting on the inner surface of the transducer. The bubbles were continually formed at the dewar walls and at the transducer during application of power. In this configuration the transducer was supported on the outer hemispherical surface at two points by TeflonTM and at a third point by

a gold electrical contact. Electrical connections were made with fine magnet wire, soldered to the silver electrodes of the piezoelectric ceramic with 52% indium, 48% tin solder. Again, care was taken to minimize acoustic radiation into the connections and supporting structure. Two grooves were cut radially into the rim so that the focal zone, which lies half below the rim, would be visible (Fig. 6).

The circuit for powering the piezoelectric transducer is presented in Fig. 7. The Tektronix FG 501A function generator was gated on and off with a gate pulse typically 1 millisecond in duration. Several seconds were allowed to elapse between gate pulses to prevent warming of the bath and the transducer. The gated sinusoidal signal was amplified to provide up to 20 watts of power, followed by a step up transformer to provide impedance matching between the power amplifier and the piezoelectric transducer.

A 1.5 liter dewar was constructed with transverse optical windows to allow the use of laser light to probe the cavitation zone. This design has the drawback of evaporating approximately half a liter of helium per hour, the major heat leak being along the inner glass vessel. The disadvantages of this dewar were more than compensated for by the undistorted optical path. Earlier attempts to detect bubbles by passing the laser beam through the

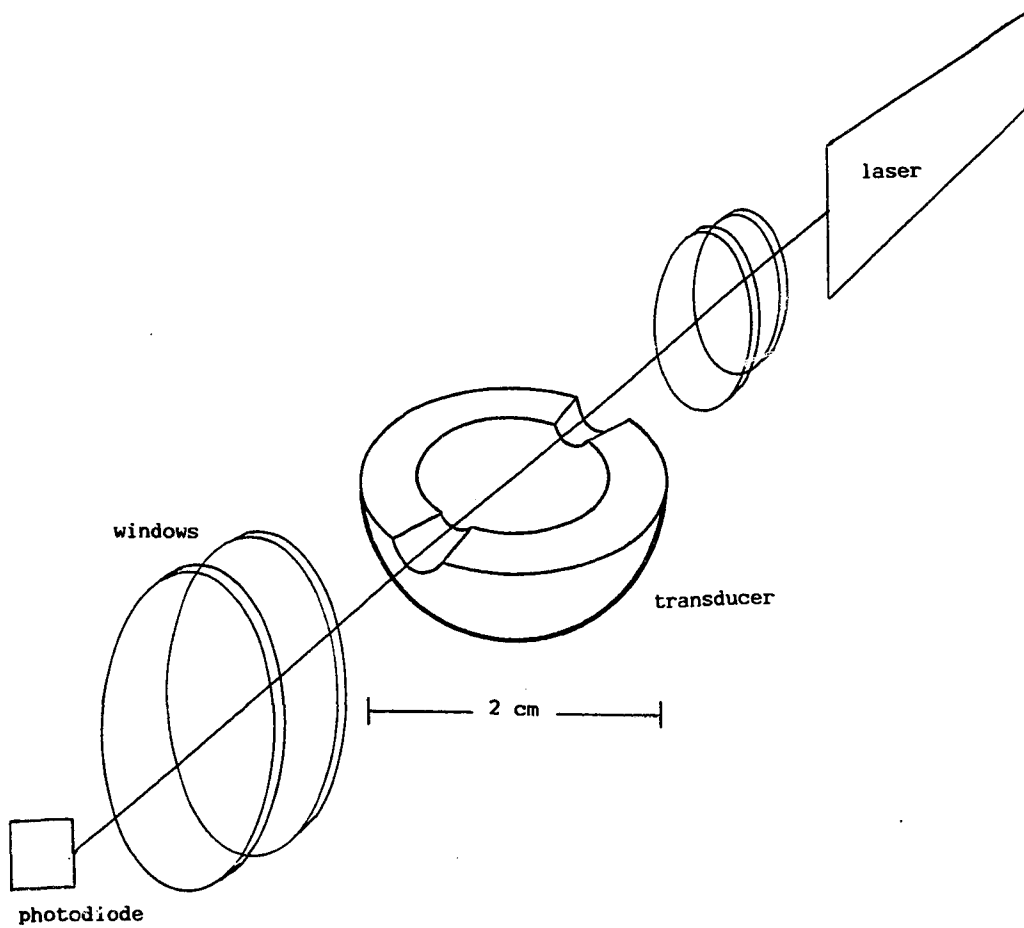


Figure 6. A schematic of the optical arrangement for detecting cavitation. When the pressure amplitude was to be measured, two cylindrical lenses were added to the optics (Fig. 19).

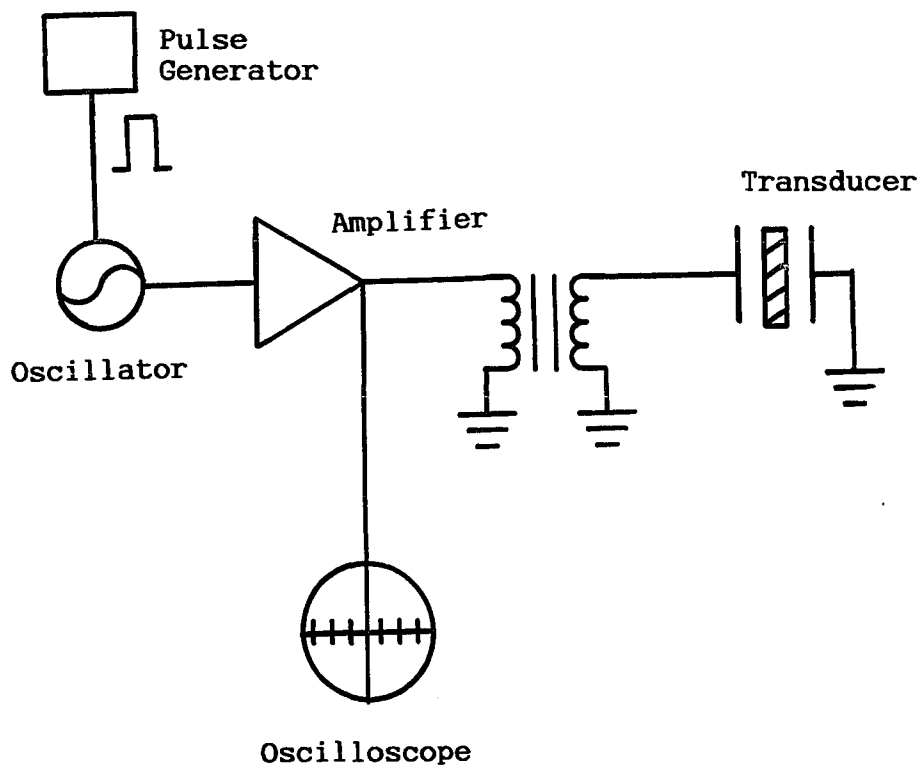


Figure 7. A schematic of the electrical circuit for powering the piezoelectric transducer.

surface of the helium were unsuccessful because of the distortions of the moving liquid surface.

The He-Ne laser was chosen to detect the onset of nucleation for three reasons. First, according to classical nucleation theory, a void in a liquid must reach a critical radius before it is energetically favorable for the bubble to grow; for ^4He , this radius is approximately 2 nm and so it is desirable to have a method of detecting very small bubbles. The extinction coefficient for light scattered from bubbles smaller than a wavelength of light is proportional to the number density of bubbles (Jackson 1975). Since there was a high density of bubbles present in the cavitation zone, light which was scattered out of the laser beam could be easily detected with a RCA 931A photomultiplier when the bubbles had grown to a radius on the order of 100 nm. Akulichev (1986) calculates that bubbles of this radius mechanically resonate at a frequency of 100 MHz. At such a high frequency it is very difficult to detect weak signals with sonic transducers. Second, the light probe has precise spatial resolution, enabling the discrimination between cavitation on the transducer's surface and at the transducer's focus. Third, the laser can be used as a pressure transducer (see Appendix B). Briefly, the pressure variations in the liquid cause periodic variations in the index of refraction, giving rise to a diffraction pattern. The

diffracted light intensity was monitored with a United Technology UDT455 photodiode configured to respond to signals with rise times shorter than a microsecond.

The helium bath pressure was monitored with an accuracy of ± 0.3 mbar by a capacitive pressure gauge (Setra Systems model 204). The bath temperature was determined to within ± 10 mK by a germanium thermometer (Lake Shore Cryogenics Inc. GR-200A-500) which was mounted at the same level as the cavitation zone. With this arrangement the temperature could be monitored while the bath was slightly overpressurized.

MEASUREMENTS

Figure 8a shows the output of the photodiode, which detects the zeroth order of the laser light diffracted from the cavitation zone. In the upper trace, the piezoelectric transducer is gated on at time zero. In 40 μ s, the sound reaches the focal point of the transducer and the light intensity drops as light is diffracted from the beam. For the next 0.4 ms, the piezoelectric transducer builds to full amplitude, after which there is no change in the light intensity. For the lower trace, the driving voltage of the piezoelectric transducer was slightly increased. More light is diffracted from the beam, and a characteristic signal appears at 0.5 msec due to cavitation. Figure 8b is an oscilloscope trace of the

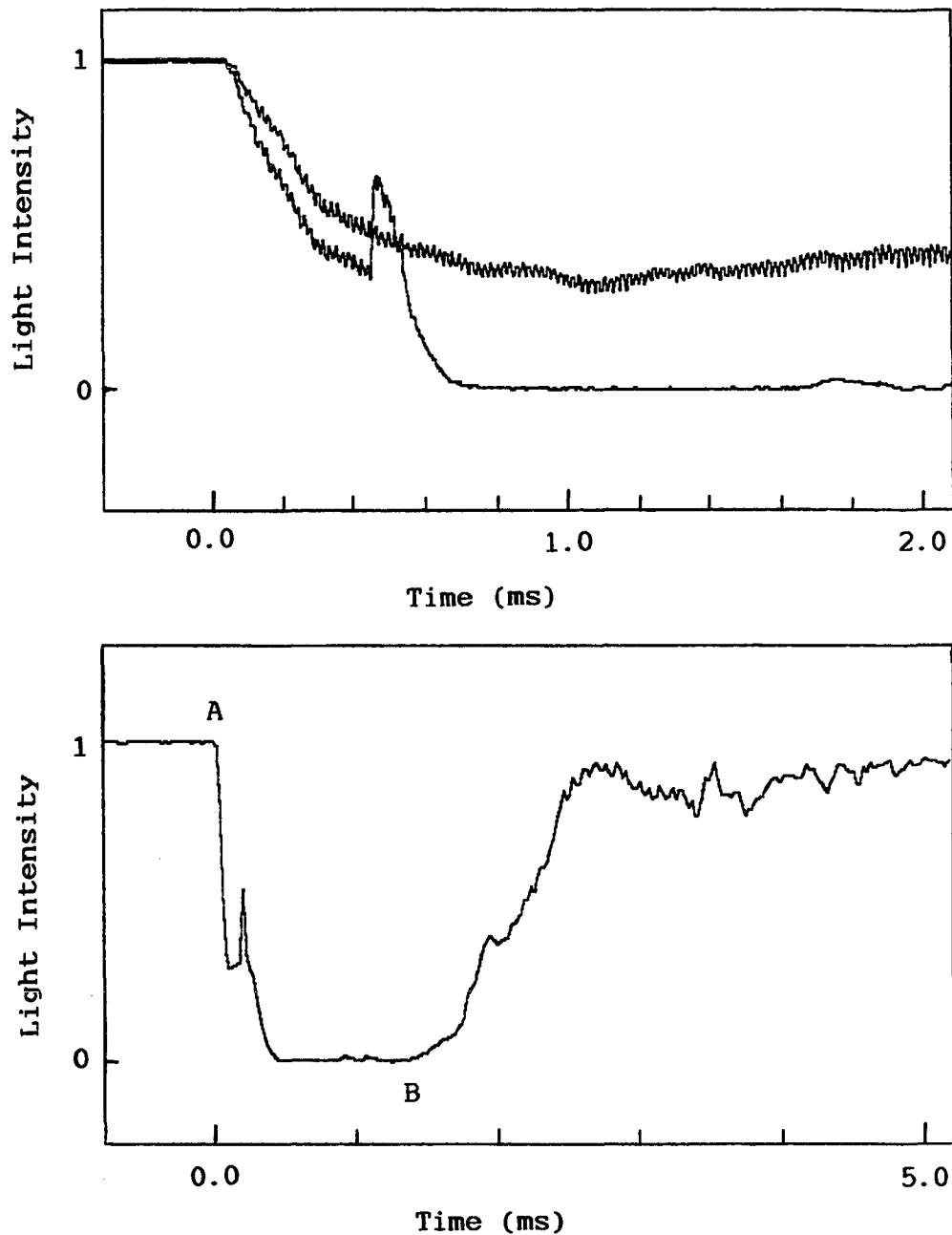


Figure 8. At $t=0$ power to the piezoelectric transducer is gated on, 40 μ sec later the sound reaches the laser beam and light is diffracted out of the central diffraction order. Upon a slight increase in the power, a characteristic peak appears due to cavitation. In the lower figure the power was turned off at point B.

large fluctuations in the light intensity that are observable at later times; the power to the transducer was turned off at point B.

Measurements of the acoustic power radiated into the liquid and of the light intensity diffracted by the ultrasound were made between 1.6 K and 4.2 K. The power to each successive gated signal was increased until the characteristic cavitation signal was observed between 0.3 and 0.5 msec from the start of the sound burst. If the delay time to the onset of cavitation was shorter than 0.3 msec, the transducer had not reached steady-state oscillation and therefore the power radiated into the liquid could not be accurately calculated. Below the lambda point, if the delay time is greater than 0.5 msec, there is the possibility that focused second sound emanating from the transducer could arrive at the cavitation zone (the speed of second sound is less than 1/10th the speed of first sound between 1.6 K and 2.17 K).

At both temperatures above 3 K, the calculation of the focal pressure from the radiated power method of Appendix A and the diffraction of light method of Appendix B were in serious disagreement. This is because at high temperatures the internal losses in the transducer are enough to cause vapor nucleation on the surface of the transducer from superheating the liquid. Bodegom (1988) found that low levels of ultrasound dramatically enhance

the nucleation rate of superheated liquid at solid surfaces. Power is therefore lost from the acoustic radiation to the growing bubbles and additionally the liquid is acoustically decoupled from the transducer. The light diffraction method of calculating the pressure amplitude at the focus is unaffected by nucleation near the surface of the piezoelectric transducer, and for this reason the method was adopted for tensile strength measurements in helium I.

OBSERVATIONS

By visually observing light scattered from the laser by bubbles in helium II, it was easily verified that light was being scattered from the focal zone of the piezoelectric transducer at the same pressure amplitudes at which light scattering was observed with the photodiode. The light scattering was visible for a fraction of a second even with a gate width of 0.5 ms. Using a spread beam and a lens, the focal zone could be projected onto a screen, on which a dark plume was visible at amplitudes corresponding to the photodiode signal.

In helium I, a similar dark plume could be seen for an instant before it was washed out by clouds of bubbles emanating from the transducer surface. These later bubbles were caused by the superheating of a thin layer of helium at the surface of the transducer as the transducer warmed due to internal losses.

High-speed photographs of the cavitation zone revealed that the cavitation and plume were fully developed within 0.5 msec of the beginning of nucleation (Fig. 9) and that the cavitation was occurring at the focus of the transducer. The 0.14 cm plume cannot be accounted for by the buoyancy of the bubbles since in 0.5 msec the buoyant force would move the bubbles an insignificant distance. It was therefore surmised that radiation pressure on the bubbles resulted in acoustic streaming of the helium within this time frame.

COMPARISON WITH THEORY

The Temperature Change

The pressure amplitude of the acoustic wave in the cavitation zone can be calculated from the methods of Appendix A or Appendix B, but in order to compare the results of the experimentally derived tensile strength with homogeneous nucleation theory, it is first necessary to determine the temperature change that accompanies the pressure change. If no shock wave is present, then the compression and rarefaction of the wave takes place adiabatically. The temperature change can be estimated from the thermodynamic relation

$$TdS = 0 = C_p dT - TV^{\alpha}_p dP \quad (5.1)$$

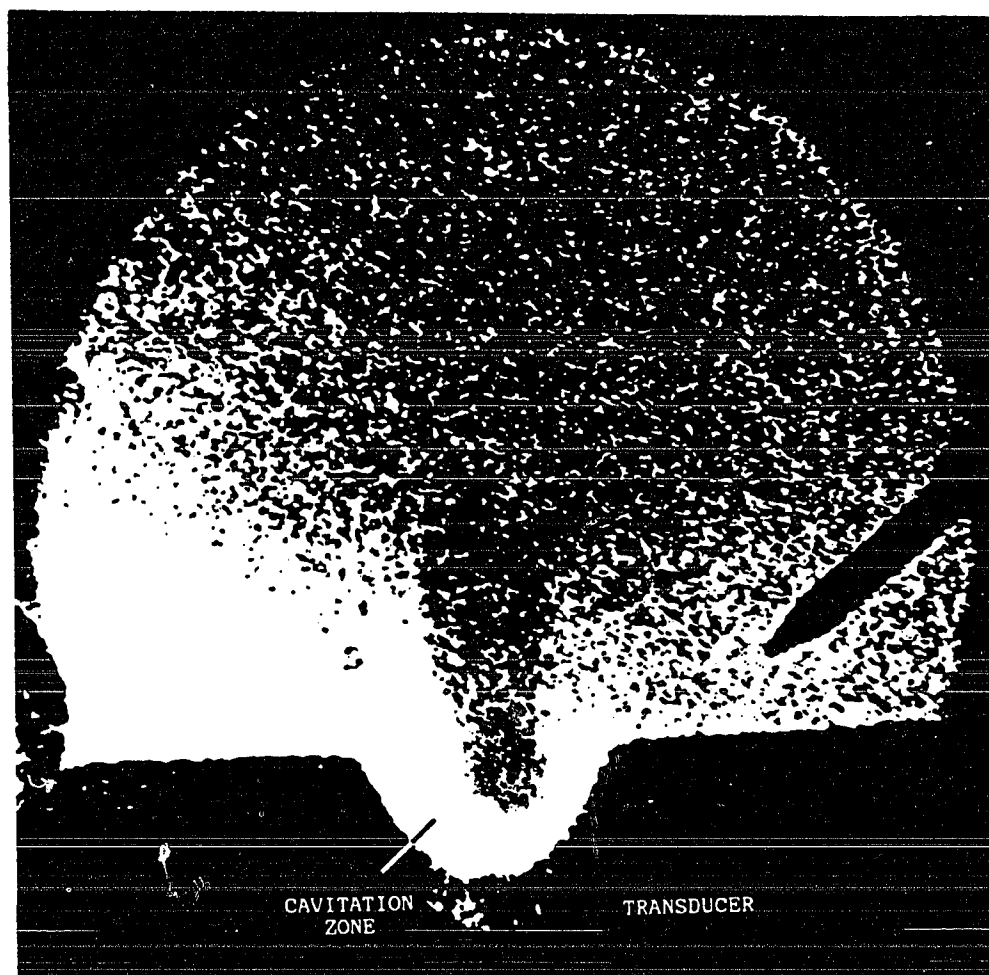


Figure 9. A photograph of the cavitation zone exposed within 0.5 msec of the initiation of cavitation.

where C_p is the specific heat capacity at constant pressure and V is the specific volume and α_p is the volume expansivity at constant pressure. Equation 5.1 can be integrated to find the temperature change if C_p and α_p are known as functions of P and T . Unfortunately, very little is known about thermodynamic variables in the metastable region. The best that can be done is to find the functional form of C_p and α_p in the stable liquid region and to extrapolate into the metastable region. It was found that the functional form of both C_p and α_p could be adequately fitted by equations of the form

$$C_p = aT^b \exp(-gP) \quad (5.2a)$$

$$V \cdot \alpha_p = \alpha T^\beta \exp(-\gamma P) \quad (5.2b)$$

where a , b , g , α , β , and γ are nearly constant for small temperature changes (see Tables I and II). The temperature change was estimated from Eqs. 5.1 and 5.2 for each data point above the lambda line. The temperature change in helium I was at most 0.4 K for the negative pressure excursions in this experiment.

TABLE I
THE PARAMETERS FOR CALCULATING THE HEAT CAPACITY
AS A FUNCTION OF PRESSURE AND TEMPERATURE
FROM EQ. 5.2A

T (K)	a (ergs/K ^b) × 10 ⁻⁶	b	g (dynes/cm ²) × 10 ⁶
2.20	153	-2.00	0.0421
2.30	154	-2.15	0.0407
2.40	155	-2.20	0.0383
2.50	153	-2.15	0.0379
2.60	157	-2.10	0.0362
2.75	2.90	+2.00	0.0344
3.00	2.71	+2.00	0.0310
3.25	2.62	+2.00	0.0410
3.50	2.59	+2.00	0.0510
3.75	2.67	+2.00	0.0786
4.00	2.85	+2.00	0.1060
4.25	3.45	+2.00	0.1960

The coefficients are based on tables of heat capacity compiled by McCarty (1973).

TABLE II
THE PARAMETERS FOR CALCULATING THE EXPANSIVITY
AS A FUNCTION OF PRESSURE AND TEMPERATURE
FROM EQ. 5.2B

T (K)	α ($\text{cm}^3/\text{T}^{\beta+1}$) $\times 10^3$	β	γ (dynes/cm^2) $\times 10^6$
2.20	1.56	5.00	0.126
2.50	3.38	5.00	0.139
2.75	2.83	4.90	0.148
3.00	2.59	4.80	0.156
3.25	2.60	4.70	0.174
3.50	2.60	4.60	0.192
3.75	2.54	4.65	0.263
4.00	2.63	4.65	0.333
4.25	2.86	4.90	0.501
4.50	2.84	5.10	0.669

The coefficients are based on tables of specific volume compiled by McCarty (1973)

Close to the lambda line, the value of the heat capacity diverges. As a result, the adiabatic temperature change becomes vanishingly small as the lambda line is approached. Below the lambda line, α_p is negative; therefore, helium II warms upon expansion and cools upon compression. The pressure excursion is, however, approximately isothermal due to the very small value of α_p in this region. No significant error will be introduced if the expansion in helium II is considered to take place isothermally in the temperature range of this experiment.

When shock waves are present in the liquid helium, additional heating due to the absorption of acoustic energy must be considered. To estimate the magnitude of the heating, it is sufficient to examine the the effect of shock waves at 1.6 K, where the acoustic amplitude is the greatest and the value of the heat capacity is the smallest. Following Rozenberg (1969), the shock wave is formed at a distance r_1 from the focus given by the equation

$$r_1 = r_0 \exp(-1/\sigma_0) \quad (5.3)$$

where r_0 is the radius of curvature of the transducer and σ_0 is given by the expression

$$\sigma_0 = \epsilon k r_0 (P_0 / \rho c_0^2)^2 \quad (5.4)$$

where ϵ is related to the nonlinearity parameter, B/A , by the expression $\epsilon = \frac{1}{2}(B/A) + 1$ (see Appendix A), k is the acoustic wave number, $2\pi/\lambda$, P_0 is the pressure amplitude at the surface of the transducer, and c_0 is the speed of sound in the unperturbed medium of density ρ .

The attenuation of the acoustic wave occurs within a hemisphere of radius r_1 . If it is assumed that the energy is absorbed uniformly by the mass of helium, m , in this hemisphere, then the temperature rise, ΔT , is given by

$$\Delta T = \Delta E/mC_p = 25 \text{ mK} \quad (5.5)$$

where ΔE is the acoustic energy absorbed by the helium during the period of shock wave production, here taken to be approximately 0.2 msec. ΔE is the difference between the acoustic energy radiated from the transducer and the acoustic energy arriving at the focal plane. Equation 5.5 is probably an overestimate of ΔT because it does not take into account the flow of cool liquid into the volume from acoustic streaming. The temperature change due to the absorption of sound is thus seen to be negligible at bath temperatures above 1.6 K.

The Nucleation Rate Far From The Lambda Transition

The results of the pressure measurements corrected for the adiabatic temperature change are graphed in Fig. 10. The data are in agreement with Becker-Doring theory for $J = 10^{15}$ critical nuclei/sec-cm³ over most of the temperature range. To see if this is reasonable, a crude estimation can be made of the rate that would be necessary to create one critical nucleus in the cavitation zone in one negative pressure excursion. For an aperture angle of 90°, the radius of the focal zone (Airy disk) is π/k where k is the wave number. The volume used in this experiment was approximately 10^{-5} cm³. In one excursion, the liquid was exposed to large negative pressures for a fraction of a microsecond. Therefore, to have a high probability of producing one bubble, J must be on the order of 10^{12} critical size bubbles/sec-cm³. This is the minimum rate for homogeneous nucleation consistent with the experimental conditions. It also must be kept in mind that in order to detect breakdown of the liquid there must be either a few large bubbles growing over many oscillations due to rectified diffusion (Akulichev 1986) or a very large number of bubbles with sizes on the order of a wavelength of light.

More information on the nucleation rate is available from the diffracted light. A closer examination of the diffracted light of Fig. 11 reveals that the moment

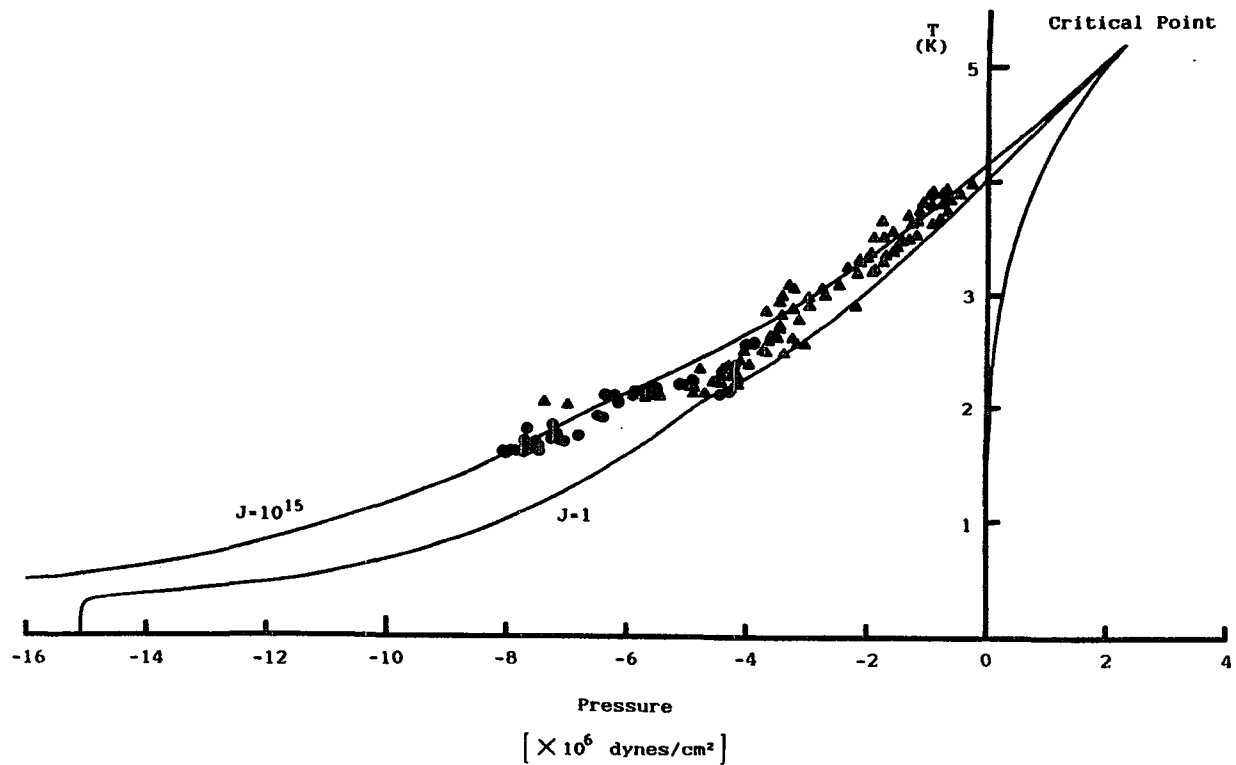


Figure 10. The experimentally obtained data agree with the theoretical homogeneous nucleation rate of $J \approx 10^{15}$ critical nuclei/sec-cm 3 . The data displayed as dots were calculated by the method of Appendix A and the data displayed as triangles were calculated by the method of Appendix B.

nucleation begins (point A), there is a dramatic increase in the light intensity of the zeroth diffraction order. Then, 10 μ sec after the start of nucleation, the light reaching the photodiode reaches a sharp maximum (point B) and decreases to undetectable levels. Curve 2 of Fig. 11 is the intensity of light scattered from the bubbles produced in the cavitation zone recorded simultaneously with the diffracted light intensity. The scattered light signal appears coincident with the sharp peak of the zeroth order diffracted light. Immediately after nucleation begins, the bubbles are too small to scatter the light, but they are absorbing power from the acoustic wave as they grow. The absorption of power manifests itself as a decrease in the acoustic pressure amplitude, causing an increase in the zeroth order light intensity. At the sharp peak in the photodiode output, the bubbles have grown large enough to scatter the laser beam, and the light intensity decreases again.

The total energy absorbed from the ultrasound during the time interval from the inception of nucleation to the beginning of significant light scattering can be estimated from the light-intensity curve. The energy absorbed from the ultrasound during the interval from A to B is on the order of 4 ergs. The energy, U , stored in a bubble of radius r which is in chemical equilibrium with the surrounding liquid is

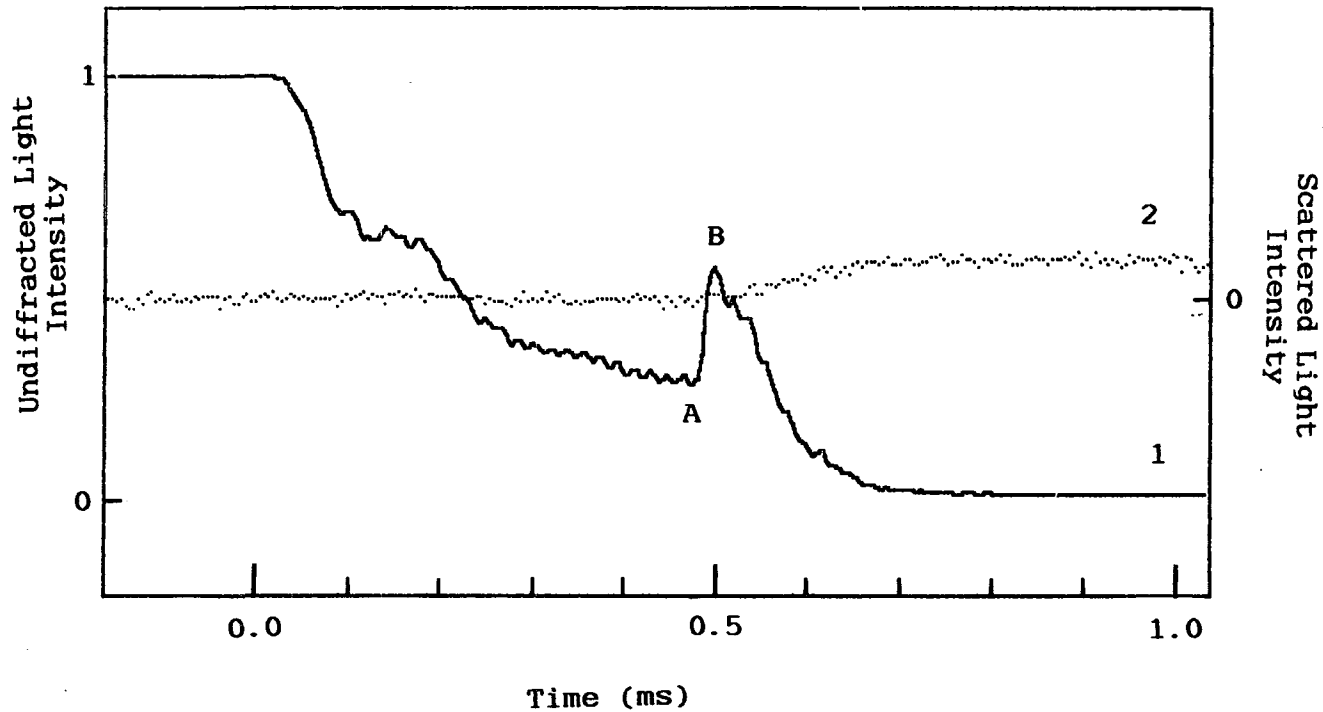


Figure 11. At point A critical size bubbles are spontaneously formed in the cavitation zone. As they grow the bubbles absorb energy from the sound beam and less light is diffracted from the zeroth order diffraction maximum. At point B the bubbles have grown large enough to scatter light out of the central diffraction maximum and the light reaching the photodiode falls to zero. Curve 2 shows the scattered light intensity.

$$U = \sigma A + (P_V - P_L)V \quad (5.6)$$

At point B the average bubble radius is on the order of the wavelength of the He-Ne laser light and $P_V - P_L$ is on the order of 3×10^6 dynes/cm². The energy stored in the average bubble is therefore on the order of 10^{-7} ergs. An estimation of the nucleation rate can now be made based on the absorbed energy, the volume of the cavitation zone and the time available for bubble formation. The result of this calculation (assuming all the critical size nuclei are formed in the first 0.1 μ sec) is a nucleation rate of $J = 10^{19}$ critical size nuclei/sec-cm³. Since part of the absorbed energy is reemitted from oscillating bubbles as random acoustic radiation and part is used in acoustic streaming and heating of the cavitation zone, this estimate should be considered an upper limit to the nucleation rate. Moreover, the shock waves emitted from oscillating bubbles are sufficient to enhance the nucleation rate once nucleation begins.

As an aside, it is interesting to note that the average rate of bubble growth can be estimated from the time delay between the inception of nucleation and the scattering of light from the bubbles. The bubbles grow to approximately 100 nm in six acoustic cycles. The bubbles only grow during the negative pressure portion of the cycle; therefore, the average radial growth rate is on the

order of 3 cm/sec.

The Nucleation Rate Near The Lambda Transition

Special consideration must be given to the nucleation rate near the lambda transition, where J decreases to approximately 1 critical nuclei/sec-cm³ (Fig. 12). This rate is in clear disagreement with the experimental conditions. Although many of the physical properties such as the speed of sound and the heat capacity are changing very rapidly near the lambda transition, the agreement of the two independent methods of determining the pressure amplitude at the focus lends credence to the effect being real rather than an artifact of the calculations.

Of the mechanisms for heterogeneous nucleation discussed in Chapter III, nucleation on quantized vortices appears to be the most likely cause of the lowered magnitude of the tensile strength. There are two theories which predict the generation of high vortex densities near the lambda transition. The first theory puts forth that excitation of larger and larger vortex rings as the lambda transition is approached is the fundamental cause of the transition from helium II to helium I (Williams 1987). In the vortex-ring model of the lambda transition, production of vortex rings is energetically unfavorable at low temperatures because of the high density of the superfluid. As the temperature is raised, the superfluid

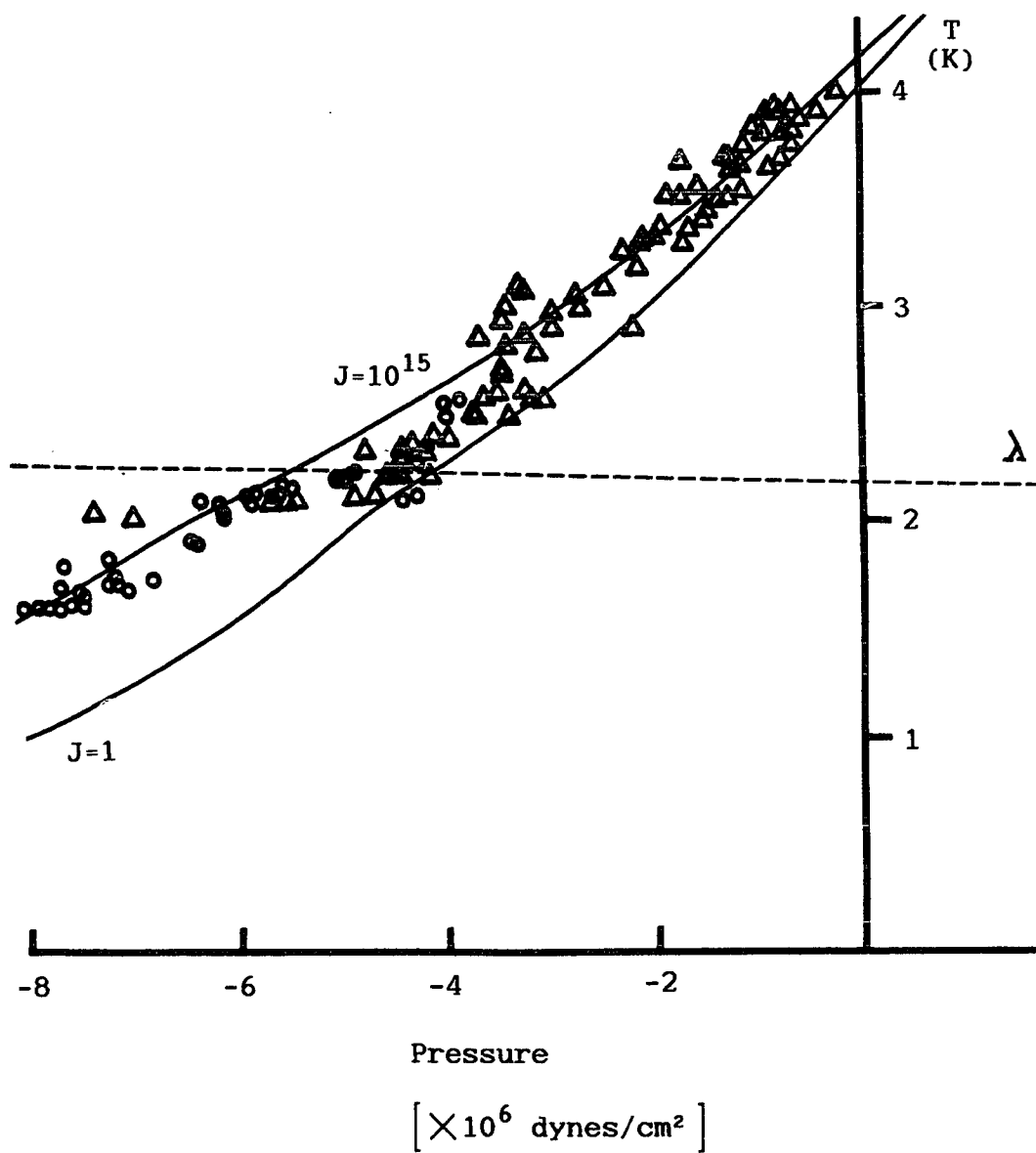


Figure 12. Near the extrapolated lambda line the nucleation rate decreases from $J = 10^{15}$ to $J = 1$ critical size nuclei/sec-cm³.

density drops and excitation of vortex rings becomes energetically favorable. This further decreases the superfluid density resulting in rings of larger radii which further decrease the superfluid density, etc. The cores of large rings are presumed to consist of smaller rings, and at the lambda transition the vortex-ring size becomes infinite. In this model, the time required to form a vortex is unimportant since the vortex rings are pre-existing in steady-state equilibrium in the unperturbed liquid.

Figure 13 plots the energy of a vortex ring, E , as a function of the ring radius (see Eq. 3.8) and the work to form a critical size bubble at 2.17 K as a function of bubble radius. The barrier height to formation of critical size bubbles for three values of J are also marked in Fig. 13. Experimentally it was observed that at the lambda transition the barrier height was lowered from its value at $J = 1$ to its value at $J = 10^{15}$ critical size nuclei/sec-cm². If vortex rings are the nucleating agents, then they must have enough energy to account for the lowered barrier height to critical size bubble formation of 1×10^{-14} ergs. The decay of any vortex ring with a radius r/a_0 greater than 6 (0.7 nm) can supply enough energy to explain the experimental result. It is also reasonable to assume that the energy density of the vortex must be greater than the energy density needed to

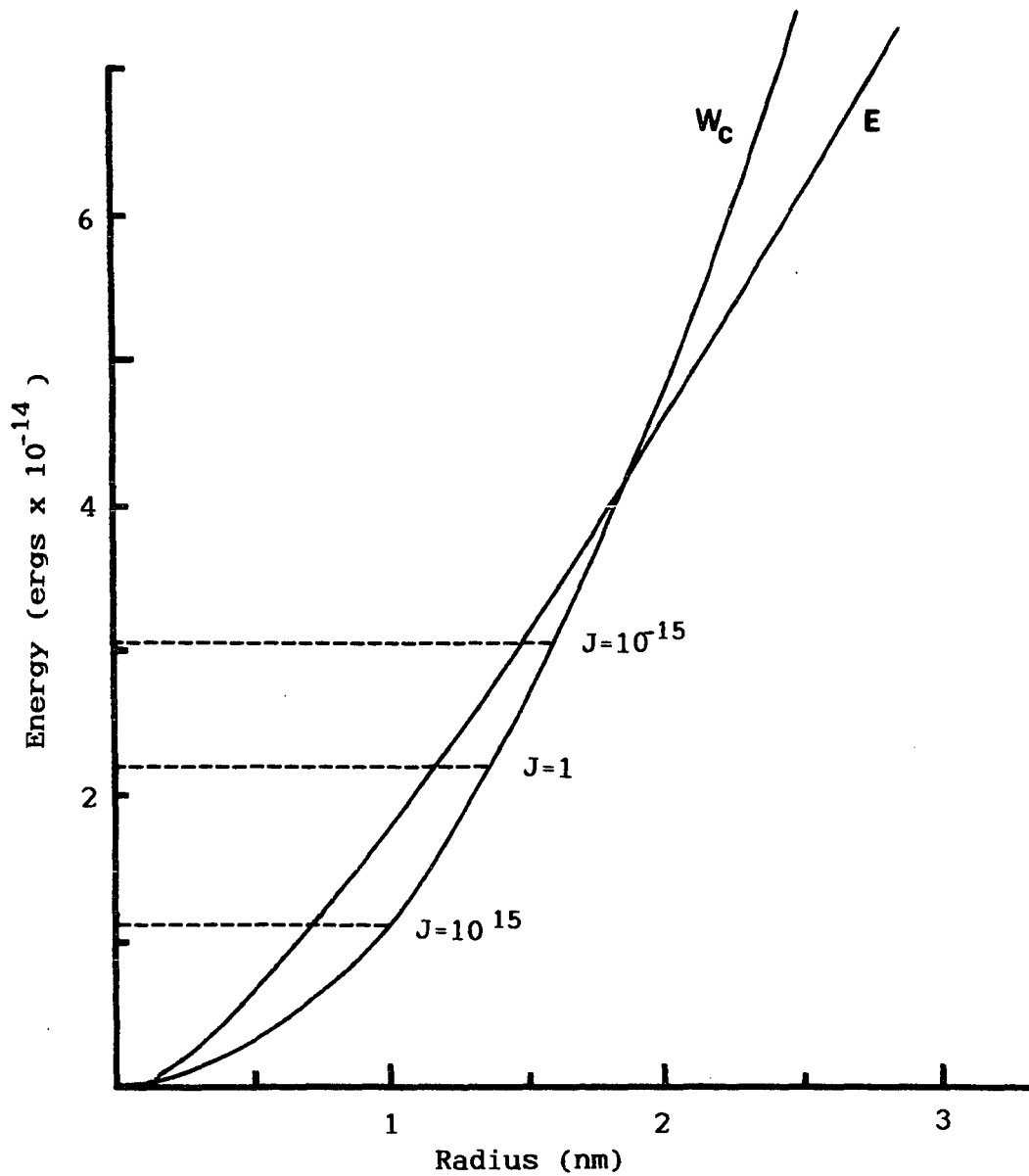


Figure 13. The work necessary to form a critical size bubble, $W_c(r)$, and the energy, $E(r)$, of a vortex ring.

form a critical size bubble. Thus the largest vortex ring capable of nucleating a bubble is given by the intersection of the two curves of Fig. 13 which occurs at 1.9 nm.

The second hypothesis for creation of vortices near the lambda transition was developed by Zurek (1985) by analogy with cosmic string theories. Zurek's mechanism for the creation of vortices requires a rapid pressure quench across the lambda line from helium I to helium II. If the transition time across the lambda line is τ_q , then the domain size, d , for causally disconnected regions is given by the following relation

$$d = \xi_0 (\tau_q / \tau_0)^{\nu/2} \quad (5.7)$$

where $\xi_0 = .56$ nm and $\nu = 1/2$ for Landau-Ginzberg theory and $\xi_0 = .40$ nm and $\nu = 2/3$ for renormalization group theory. Both theories predict $\tau_0 \approx 8.5 \times 10^{-12}$ sec. The domain size in the experiments described here would be approximately 10 nm, resulting in a vortex density of about 10^{17} vortices/cm³ of average length d . In order to explain the observed reduction in the magnitude of the tensile strength near the lambda transition, the density of bubbles formed in the 10^{-7} sec interval, during which time the liquid helium is at high negative pressures, must be less than the vortex density. Since the nucleation

rate must be approximately $J = 10^{15}$ bubbles/sec-cm³, the bubble density in each negative pressure excursion is 10^8 bubbles/cm³. Only one vortex of length d out of 10^9 needs to nucleate a bubble in order explain the reduction in the magnitude of the tensile strength near the lambda transition.

The objection might be raised that since the magnitude of the tensile strength appears to be depressed in helium I as well as helium II, quantized vortices (a superfluid phenomenon) cannot be the heterogeneous nucleation mechanism. However, if it is hypothesized that small inclusions of superfluid exist in helium I at temperatures close to the lambda line, then there is no conflict with the experimental results. The idea that statistical temperature fluctuations lead to small inclusions of superfluid in helium I was used by Keesom (1935) to explain the anomalous heat capacity and by Pippard (1951) to explain the attenuation of sound at temperatures just above the lambda transition. Pippard estimates that at 2.3 K, ten percent of the liquid density consists of inclusions of superfluid in clusters of on the average 850 atoms. Superfluid inclusions of this size are larger than a critical size nucleus.

CHAPTER VI

SUMMARY AND CONCLUSION

Although liquid helium is in many respects the closest liquid to an ideal fluid for tensile strength measurements, the failure of previous experiments to reach the theoretical value of the tensile strength suggests that a careful examination of mechanisms for heterogeneous nucleation must be pursued. In the first half of this thesis, known and suspected causes of heterogeneous nucleation in helium were enumerated and a strategy was presented to increase the probability of observing homogeneous nucleation. Central to this strategy is the minimization of solid surfaces in regions of negative pressure. It was also argued that homogeneous nucleation is likely to be the dominant nucleation mechanism only for rapid and deep excursions into the metastable region. Under these conditions an explosive production of bubbles should signal the onset of homogeneous nucleation, the production of a few isolated bubbles is likely to be caused by heterogeneous nucleation. In this way bubbles nucleated heterogeneously can usually be distinguished from bubbles nucleated in the homogeneous liquid.

The realization of these ideas was accomplished with

the use of high-frequency focused ultrasound. This method has the advantage of fast excursions into the metastable region as well as the advantage of placing high-amplitude pressure variations far from container walls. The problem of measuring the acoustic pressure amplitude in a small focal region was attacked in two ways. At low temperatures the pressure amplitude was calculated from the acoustic power radiated into the liquid. In order to verify this calculation and to extend the measurements to higher temperatures, a new theory for the diffraction of light from highly-focused ultrasound was developed.

The experimental results of the tensile strength measurements were consistent with the theoretical homogeneous nucleation rate of $J = 10^{15}$ critical size nuclei/sec-cm³ over most of the temperature range investigated (1.6 K - 4.0 K). Near the lambda transition a significant lowering of the magnitude of the tensile strength was observed. This lowering of the magnitude of the tensile strength is inconsistent with homogeneous nucleation and it was proposed that the production of quantized vortices associated with the lambda transition could explain the experimental results.

Finally, the results of this experiment can be compared with the results of measurements of homogeneous nucleation for all other liquids. The curves of homogeneous nucleation for most liquids lie on a universal

set of curves if the homogeneous nucleation curves are plotted in terms of the reduced pressure, P/P_C , and the reduced temperature, T/T_C . For liquids with a high de Boer parameter, Λ , like liquid helium, however, a quantum mechanical corresponding states analysis must be employed. Sinha (1982) found that the quantum mechanical universal homogeneous nucleation curves could be represented by the equation

$$(1 - T/T_C) = m(\Lambda)(1 - P/P_C)^{n(\Lambda)} \quad (6.1)$$

where $m = 0.22$ and $n = 1.001$ for ${}^4\text{He}$ while $m = 0.14$ and $n = 0.922$ for classical liquids such as argon. This comparison reveals that in the negative pressure region, homogeneous nucleation theory now has been confirmed over a range three times greater for liquid helium than for any liquid studied previously.

REFERENCES

- Akulichev, V.A., "Acoustic Cavitation in Low-Temperature Liquids," *Ultrasonics* 26, 8-18 (1986).
- Akulichev, V.A., and V.A. Bulanov, "Strength of Quantum Liquids," *Sov. Phys. Acoust.* 20, 501-503 (1975).
- Apfel, R.E., "A Novel Technique for Measuring the Strength of Liquids," *J. Acoust. Soc. Am.* 49, 145-155 (1971).
- Beams, J.W., "Tensile Strength of Liquid Helium II," *Phys. Rev.* 104, 880-882 (1956).
- Beams, J.W., "Tensile Strengths of Liquid Argon, Helium, Nitrogen, and Oxygen," *Physics of Fluids* 2, 1-3 (1959).
- Beyer, R.T., "Nonlinear Acoustics," in Physical Acoustics, edited by W.P. Mason (Academic Press, New York, NY 1965) Chap. 10, pp. 231-263.
- Blander, M., and J.L. Katz, "Bubble Nucleation in Liquids," *AIChE Journal* 21, 833-848 (1975).
- Brown, R.C.A., H.J. Hilke, and A.H. Rogers, "Ultrasonic Helium Bubble Chamber," *Nature* 220, 1177-1178 (1968).
- Bodegom, E., J.A. Nissen, L.C. Brodie, and J.S. Semura, "Sound Induced Enhancement of Heat Transfer from a Solid into Liquid Helium," *Advances in Cryog. Eng.* 33, 349-355 (1988).
- Carey, R.F., J.A. Rooney, and C.W. Smith, "Subharmonic Responses in Liquid Helium," *J. Acoust. Soc. Am.* 66, 1801-1806 (1979).
- Cook B.D., "Optical method for ultrasonic waveform analysis, using a recursion relation," *J. Acoust. Soc. Am.* 37, 172-173 (1965).
- De Yoreo, J.J., and R.O. Pohl, "Low-Temperature Thermal Properties of Ferroelectrics," *Phys. Rev. B* 32, 5780-5784 (1985).

- Dhingra, H.C., and R.D. Finch, "Experiments on Ultrasonic Cavitation in Liquid Helium in the Presence of Second Sound," *J. Acoust. Soc. Am.* 59, 19-23 (1976).
- Edwards, M.H., R.M. Cleary, and W.M. Fairbank, "Bubble Formation on Vortices in a Liquid Helium Bubble Chamber," in Quantum Fluids, edited by D.F. Brewer North-Holland Publishing Co., Amsterdam, 1966), p. 140-143.
- Finch, R.D., R. Kagiwada, M. Barmatz, and I. Rudnick, "Cavitation in Liquid Helium," *Phys. Rev. A* 134, 1425-1428 (1964).
- Finch, R.D., and T.G. Wang, "Visible Cavitation in Liquid Helium," *J. Acoust. Soc. Am.* 3, 511-514 (1966).
- Finch, R.D., T.G. Wang, R. Kagiwada, M. Barmatz, and I. Rudnick, "Studies of the Threshold-of-Cavitation Noise in Liquid Helium," *J. Acoust. Soc. Am.* 40, 211-218 (1966).
- Finch, R.D., and M.L. Chu, Jr., "Production and Detection of Solitary Macroscopic Quantized Vortices in Helium II," *Phys. Rev.* 161, 202-206 (1967).
- Good, R.J., and G.V. Ferry, "The Wetting of Solids by Liquid Hydrogen," *Adv. Cry. Eng.* 8, 306-310 (1962).
- Gottlieb M., "Elasto-optic Materials," in Handbook of Laser Science and Technology, (CRC Press, Boca Raton, Florida, 1986), Section 2, pp. 319-341.
- Hadi, Z.E., M. Durieux, and H. Van Dijk, "The Density of Liquid ^4He Under its Saturated Vapor Pressure," *Physica* 41, 289-304 (1969).
- Hikata, A., H. Kwun, and C. Elbaum, "Finite Amplitude Wave Propagation in Solid and Liquid ^4He ," *Phys. Rev. B* 21, 3932-3940 (1980).
- Jackson, J.D., Classical Electrodynamics (John Wiley & Sons, New York, NY, 1975), 2nd ed., Chap. 9, pp. 411-423.
- Jarman, P.D., and K.J. Taylor, "Sonically Induced Cavitation of Liquid Helium," *J. Low Temp. Phys.* 2, 389-402 (1970).

- Kashkooli, H.A., P.J. Dolan, Jr., and C.W. Smith,
"Measurement of the Acoustic Nonlinearity Parameter
in Water, Methanol, Liquid Nitrogen, and Liquid
Helium-II by Two Different Methods: A Comparison," J.
Acoust. Soc. Am. 82, 2086-2089 (1987).
- Keesom, W.H., and A.P. Keesom, "Specific Heat of Liquid
Helium," Physica 2, 557-565 (1935).
- Kerr, E.C., and R.D. Taylor, "The Molar Volume and
Expansion Coefficient of Liquid He⁴," Ann. Phys. 26,
292-306 (1964).
- King, A.L., "The Spore Discharge Mechanisms of Common
Ferns," Proc. N.A.S. 30, 155-161 (1944).
- Klein, W.R., and B.D. Cook, "Unified Approach to Ultrasonic
Light Diffraction," IEEE Trans. Sonics and
Ultrasonics (SU) 14, 123-134 (1976).
- Leroy O., and J. M. Claeys, "Diffraction of light by
profiled ultrasound," Acoustica 55, 21-25 (1984).
- Lifshitz, I.M., and Yu. Kagan, "Quantum Kinetics of Phase
Transitions at Temperatures Close to Absolute Zero,"
Zh. Eksp. Teor. Fiz. 62, 385-402 (1972).
- Marston, P.L., "Tensile Strength and Visible Ultrasonic
Cavitation of Superfluid ⁴He," J. Low Temp. Phys. 25,
383-407 (1976).
- Mate, C.F., and K.L. McCloud, "Stability and Rupture of
Helium at Negative Pressures: Anomalous Vapor Phase
Nucleation," in Proc. 11th Int. Conf. Low Temp.
Phys., edited by J.F. Allen, (U. of St. Andrews
Press, 1968), pp. 308-317.
- McCarty, R.D., "Thermophysical Properties of Helium-4 from
2 to 1500 K with Pressures to 10⁸ Pa," J. Phys. Chem.
Ref. Data, 2, 923-1041 (1973).
- McConnell, P.M., M.L. Chu, Jr., and R.D. Finch,
"Mechanism of Ultrasonic Cavitation Nucleation in
Liquid Helium by Quantized Vortices," Phys. Rev. A 1,
411-418 (1970).
- Misener, A.D., and G.R. Herbert, "Tensile Strength of
Liquid Helium II," Nature 177, 946-947 (1956).

- Mosse, A., M.L. Chu, Jr., and R.D. Finch, "Movie Films of Cavitation in Superfluid Helium," J. Acoust. Soc. Am. 47, 1258-1261 (1970).
- Mosse, A., and R.D. Finch, "Spectral Analysis of Cavitation Noise in Cryogenic Liquids," J. Acoust. Soc. Am. 49, 156-165 (1971).
- Nagai S., "Acoustic power measurements of focused waves: Radiation force and Raman-Nath methods," J. Acoust. Soc. Jpn. (E) 7, 4, 229-231 (1986).
- Nauagol'nykh, K.A., "Absorption of Finite-Amplitude Waves," in High-Intensity Ultrasonic Fields, edited by L.D. Rozenberg (Plenum Press, New York, NY 1971) Part 1, pp. 3-75.
- Neppiras, E.A., and R.D. Finch, "Acoustic Cavitation in Helium, Nitrogen, and Water at 10 kHz," J. Acoust. Soc. Am. 52, 335-343 (1971).
- Nissen J.A., E. Rodegom, L.C. Brodie, and J. S. Semura, "New measurements of the tensile strength of ⁴He," Advances in Cryog. Eng. 33, 999-1003 (1988)
- Pippard, A.B., "Ultrasonic Propagation in Liquid Helium near the Lambda-Point," Phil. Mag. 42, 1209-1223 (1951).
- Rozenberg, L.D., "Ultrasonic Focusing Radiators," in Sources of High-Intensity Ultrasound, edited by L.D. Rozenberg (Plenum Press, New York, NY 1969), Vol. 1, pp. 223-305.
- Sapriel J., in Acousto-Optics, (Wiley and Sons, Chichester New York, 1976), Chap. VI, pp. 54-60.
- Shadley, J.R., and R.D. Finch, "Nucleation of Ultrasonic Cavitation by Alpha-Particle Irradiation of Liquid Helium," Phys. Rev. A 3, 780-785 (1971).
- Scholander, P.F., "Tensile Water," Amer. Scientist 60, 584-590 (1972).
- Scholander, P.F., H.T. Hammel, E.D. Bradstreet, and E.A. Hemmingsen, "Sap Pressure in Vascular Plants," Science 148, 339-346 (1965).
- Sinha, D.N., PhD. Thesis, Portland State University, (1980).

- Sinha, D.N., J.S. Semura, and L.C. Brodie, "Homogeneous Nucleation in ^4He : A Corresponding-States Analysis," *Phys. Rev. A* 26, 1048-1061 (1982).
- Skripov, V.P., Metastable Liquids, (John Wiley & Sons, New York, NY 1974), Chaps. 1-7, pp. 1-191.
- Smith, C.W., M.J. Tejwani, and D.A. Farris, "Bifurcation Universality for First-Sound Subharmonic Generation in Superfluid Helium-4," *Amer. Phys. Soc.* 48, 492-494 (1982).
- Smith, C.W., and M.J. Tejwani, "Bifurcation and the Universal Sequence for First-Sound Subharmonic Generation in Superfluid Helium-4," *Physica* 7D, 85-88 (1983).
- Thormahlen, I., "Superheating of Liquids at the Onset of Boiling," *Proc. 8th Internat. Heat Transfer Conf.*, 2001-2006 (1986).
- Vignos, J.H., and H.A. Fairbank, "Sound Measurements in Liquid and Solid He^3 , He^4 , and He^3 - He^4 Mixtures," *Phys. Rev.* 147, 185-190 (1966).
- Vinen, W.F., "Mutual Friction in a Heat Current in Liquid Helium II I. Experiments on Steady Heat Currents," *Proc. Royal Soc.* A240 114-127 (1957).
- Vinen, W.F., "Mutual Friction in a Heat Current in Liquid Helium II II. Experiments on Transient Effects," *Proc. Royal Soc.* A240 128-143 (1957).
- Volmer, M. and A. Weber, "Nucleus Formation in Supersaturated Systems," *Z. Phys. Chem.* 119, 277 (1926).
- Wilks, J., The Properties of Liquid and Solid Helium, (Clarendon Press, Oxford, 1967) Appendix A1, p. 666.
- Williams, G.A., "Vortex-Ring Model of the Superfluid λ Transition," *Phys. Rev. Lett.* 59, 1926-1929 (1987).
- Wilson, M.F., D.O. Edwards, and J.T. Tough, "Osmotic Pressure of Dilute He^3 - He^4 Solutions and the Tensile Strength of Liquid He II," *Bull. Am. Phys. Soc.* 12, 96 (1967).

Zankel K.L., and E. A. Hiedemann, "Diffraction of light by ultrasonic waves progressing with finite but moderate amplitudes in liquids," J. Acoust. Soc. Am. 31, 44-54 (1959).

Zurek, W.H., "Cosmological Experiments in Superfluid Helium?," Nature 317, 505-508 (1985).

APPENDIX A

CALCULATION OF THE FOCAL PRESSURE FROM THE RADIATED POWER

THE POWER RADIATED INTO THE LIQUID

To determine the power radiated into the liquid, measurements of the electrical impedance of the piezoelectric transducer were made with the circuit of Fig. 14, both with the transducer in the helium bath and with it suspended just above the liquid surface. The electrical impedance, $Z(\omega)$, is calculated from the equation of a voltage divider

$$Z(\omega) = R \cdot (V_i/V_o - 1) \quad (A1)$$

where V_i and V_o are the input and output voltages of the voltage divider formed by the transducer and the resistance R . At the series resonant frequency, ω_o , the impedance is a minimum.

In order to determine the pressure amplitude at the surface of the transducer, the piezoelectric transducer was modeled after the equivalent circuit (Fig. 15) for a piezoelectric plate operating at its series resonance frequency. The circuit of Fig. 15 is easily utilized for

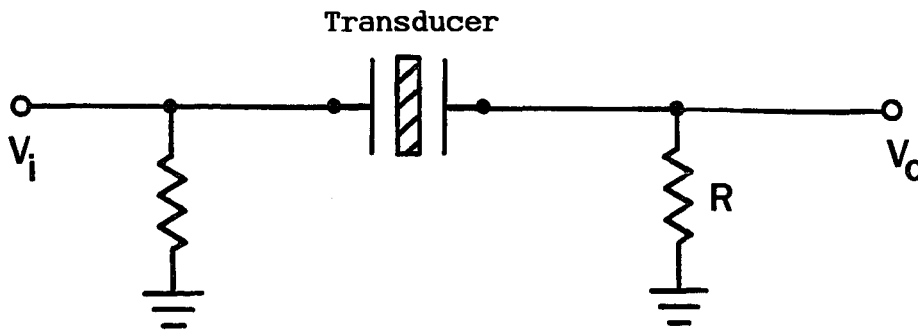


Figure 14. Schematic of the circuit used to measure the impedance of the piezoelectric transducer.

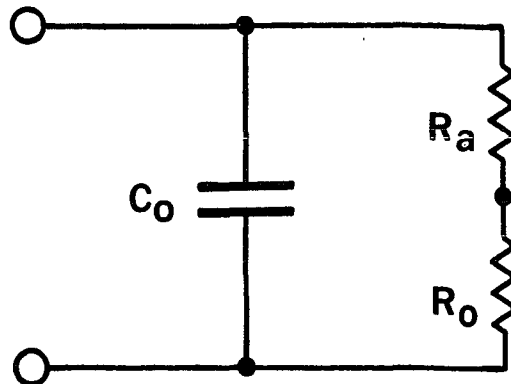


Figure 15. The equivalent circuit for a piezoelectric plate operated at its series resonance. C_0 represents the electrical capacitance, R_0 and R_a represent the internal and radiation losses respectively.

making power measurements. The electrical impedance, $Z(\omega_0)$, of the transducer at its resonant frequency was measured while the piezoelectric cell was submerged in the liquid helium. From the impedance, the resistance $R_T = R_a + R_0$ can be calculated using the equivalent circuit

$$R_T = |Z(\omega_0)| \left[1 - \left(\omega_0 C_0 |Z(\omega_0)| \right)^2 \right]^{-\frac{1}{2}} \quad (A2)$$

where $C_0 = 300$ pF is the capacitance formed by the dielectric material and the electrodes of the transducer. R_a represents the resistance to the power radiated into the liquid, which is the quantity sought. R_0 , which represents internal losses in the piezoelectric ceramic and acoustic losses into the supports, was obtained by measuring the electrical impedance of the transducer at resonance while the transducer was suspended above the liquid. Under these conditions, R_T equals R_0 . It is necessary to maintain the transducer at the same temperature when measuring the total and internal impedances; therefore, the resonant frequency, which is temperature dependent, was monitored and the transducer was cooled if the frequency drifted. This was the greatest source of experimental error in the measurements. Using this method, R_T and R_0 were found to be about 75 Ω

and 57 Ω respectively. The total acoustic power radiated into the liquid was calculated from the equivalent circuit and the voltage amplitude at the piezoelectric transducer's terminals. It can easily be shown that

$$I \cdot S = \frac{R_a}{2R_T^2} V^2 \quad (A3)$$

where I is the acoustic intensity, S is the area of the radiating surfaces and V is the voltage amplitude. Since the acoustic intensity for a spherical wave inside the piezoelectric ceramic is inversely proportional to r^2 , equal power is radiated from the inner and outer faces of the transducer.

THE PRESSURE AMPLITUDE AT THE FOCUS

The Pressure Amplitude At The Surface

The pressure amplitude, P_0 , at the surface of the transducer can now be calculated using the relation between the pressure amplitude of a sinusoidal acoustic wave and the acoustic intensity

$$I_0 = P_0^2 / 2\rho c_0 \quad (A4)$$

where c_0 is the speed of sound in the liquid of density ρ . This expression is valid for both plane waves and

spherical waves.

The pressure amplitude at the focus of a spherical focusing transducer with uniform pressure amplitude at the radiating face can be calculated from geometrical considerations

$$P_f = P_o k F(1 - \cos \alpha_m) \quad (A5)$$

where k is the acoustic wave number, $2\pi/\lambda$, and F is the focal length of the transducer and α_m is the half aperture angle. Equation A5 is valid for small amplitudes and ignores the linear absorption of sound.

In liquid helium, the linear absorption of sound is insignificant in traveling from the transducer surface to the focal zone for the experimental setup. However, when the intensity of the wave becomes sufficiently large, strong nonlinear absorption of sound occurs and Eq. A1 is no longer valid.

The Acoustic Nonlinearity Parameter

The quantity B/A is known as the acoustic nonlinearity parameter and plays a central role in determining both the absorption and the distortion of a finite-amplitude acoustic wave (Beyer 1965)

$$\frac{B}{A} = \frac{\rho_o}{c_o^2} \left(\frac{\delta^2 p}{\delta \rho^2} \right)_{s, \rho = \rho_o} \quad (A6)$$

where the derivative is evaluated at constant entropy. B/A has been measured directly for a number of liquids including liquid helium. Kashkooli et.al. (1987) measured the nonlinearity parameter at 1.8 K both by an optical method and by a finite loss method. They found $B/A \approx 4$ on the saturation curve. Hikata et.al. (1980) found that near the solidification curve, the theoretical value of $B/A = 3.7$ was consistent with their measurements in helium II. B/A can also be evaluated from the thermophysical properties of helium. Equation A6 is inconvenient for this purpose and an alternative form utilizing first order derivatives can be used in its place

$$\frac{B}{A} = 2\alpha_0 c_0 \left(\frac{\delta c}{\delta P} \right)_T + 2c_0 \frac{T\alpha}{C_p} \left(\frac{\delta c}{\delta T} \right)_P \quad (A7)$$

where α is the expansivity and C_p is the specific heat at constant pressure. The calculated values are presented in Table III for selected temperatures.

The Pressure Amplitude At The Focus

Following Rozenberg (1969), the pressure amplitude at the focus is given by

$$P_f' = \frac{\pi P_0 K_p}{\pi - 1 + (\epsilon K_p P_0 / \rho c_0^2) \ln K_p} \quad (A8)$$

TABLE III
THE NONLINEARITY PARAMETER B/A

T (K)	$\left(\frac{\partial c}{\partial P}\right)_T$ cm ³ sec/g × 10 ⁴	$\left(\frac{\partial c}{\partial T}\right)_P$ cm/sec-K × 10 ⁻³	$\frac{B}{A}$
1.25	8.51 ± 0.5	-1.19 ± 0.7	5.9 ± 0.4
1.50	8.79 ± 0.8	-1.20 ± 0.4	5.9 ± 0.4
1.75	7.87 ± 0.4	-1.49 ± 0.1	5.4 ± 0.3
1.80	7.89 ± 0.4	-1.84 ± 0.1	5.4 ± 0.3
1.90	8.26 ± 0.3	-2.68 ± 0.2	5.6 ± 0.3
2.00	8.19 ± 0.4	-3.74 ± 0.1	5.5 ± 0.3
2.10	7.63 ± 0.5	-4.99 ± 0.6	5.0 ± 0.3
2.20	8.67 ± 0.2	+2.08 ± 0.5	5.6 ± 0.2
2.25	9.03 ± 0.1	+1.41 ± 0.2	5.9 ± 0.2
2.50	9.28 ± 0.1	-0.13 ± 0.3	5.9 ± 0.3
3.00	10.05 ± 0.1	-1.93 ± 0.1	5.7 ± 0.1
3.50	12.20 ± 0.1	-3.45 ± 0.2	5.3 ± 0.3
4.00	15.48 ± 0.1	-5.60 ± 0.2	5.1 ± 0.2
4.20	17.80 ± 0.1	-6.89 ± 0.1	5.1 ± 0.4

This table is based on the speed of sound measurements of Vignos (1966), the expansivity measurements of Kerr (1964), the density measurements of Hadi (1969), the heat capacity compiled by McCarty (1972) and Wilks (1967).

where $K_p = kF(1 - \cos \alpha_m)$ and $\epsilon = \frac{1}{2}(B/A) + 1$. This relation is valid under the condition that shock waves are present; that is, when

$$(\epsilon K_p \rho_0 / \rho c_0^2) \ln K_p \geq 1 \quad (\text{A9})$$

Internal Losses

The internal losses of the piezoelectric transducer can also be calculated from the electrical impedance measurement

$$H = \frac{R_0}{2R_T} v^2 \quad (\text{A10})$$

where H is the power dissipated as Joule heating. It is not possible to separate losses due to heating and losses due to acoustic radiation into the supporting structure, but it is reasonable to suppose that the radiation into the support was negligible since R_0 was fairly constant for different support structures. From Eqs. A3, A10 and the values of R_a and R_0 it is apparent that almost four times more power goes into heating the transducer than into the helium in the form of acoustic radiation. This result is to be expected because of the poor acoustic impedance match between liquid helium and solids.

It is interesting to note that due in part to the low

heat capacity of the piezoelectric material at low temperature (De Yoreo 1985), the heat fluxes used in the ⁴He tensile strength are enough to superheat the liquid at the surface of the transducer. At bath temperatures above about 3 K, bubble nucleation on the surface of the heated transducer did significantly reduce the coupling between the transducer and the liquid helium.

APPENDIX B

INTRODUCTION

This study of light diffraction from ultrasound was motivated by cavitation studies of liquid helium in which the ultrasound was highly focused in order to attain the maximum tensile strength of the liquid. In these investigations it was necessary to know the acoustic pressure amplitude at the focus of the sound beam. For a highly focused system where the diameter of the focal zone is on the order of an acoustic wavelength, any detector placed near the focus must be small compared to a wavelength in order to resolve the central diffraction maximum. Furthermore, if the detector is made from a material substance it will disturb the acoustic field under investigation. In the case of cavitation studies, a solid probe will also act as a site for heterogeneous nucleation.

The advantage of an optical method for detecting ultrasound lies in its ability to detect the presence of the sound without disturbing the sound field. The Raman-Nath approach for the diffraction of light from ultrasonic waves also has the benefit of providing an absolute measurement of the pressure amplitude (Klein 1976, Sapriel

1976, Gottlieb 1986). It has been shown (Nagai 1986) that the Raman-Nath method even for small curvature of the phase fronts leads to large errors. For strongly focused sound, therefore, this method needs to be modified.

THEORY

Diffraction from a profiled sound beam

In the Raman-Nath approximation, density variations due to a thin beam of ultrasound create an optical phase grating. In the simplest case, light is incident at right angles to the propagation vector of the sound (Fig.16). The intensity of the n th order diffracted light can be shown to be proportional to the square of the n th order Bessel function

$$I_n \propto J_n^2(v), \quad (B1)$$

where v is the Raman-Nath parameter, which can be expressed as

$$v = \frac{\pi l n^3}{\lambda c_0^2} \left(\frac{\delta n}{\delta \rho} \right)_S P, \quad (B2)$$

where the derivative is taken at constant entropy, λ is the wavelength of light in a vacuum, and c_0 is the speed of sound in the medium with density ρ and index of

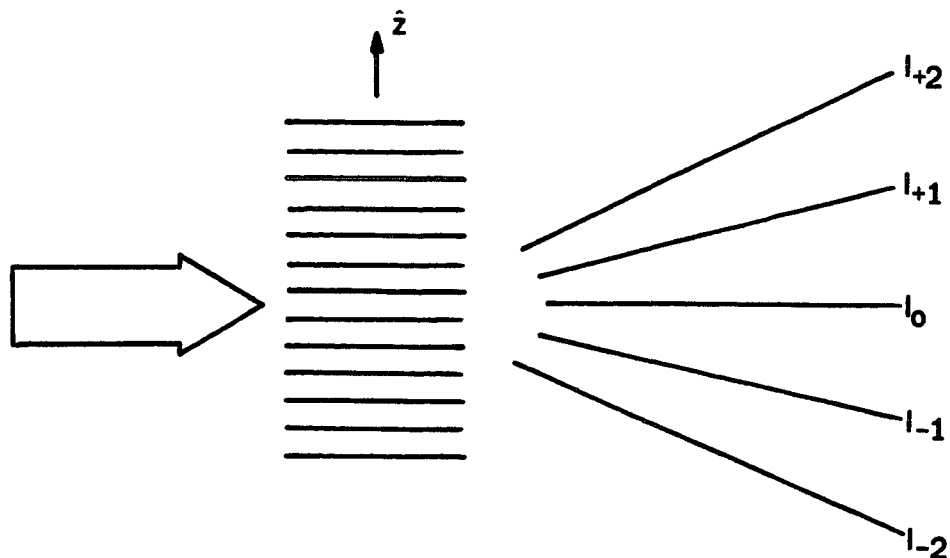


Figure 16. A uniform acoustic beam with propagation vector in the z direction diffracts light incident from the left into discrete diffraction orders. If the pressure varies sinusoidally and the beam width, l , is narrow then the intensity of the n th diffraction order is proportional to the square of the n th order Bessel function.

refraction n . The parameter l is the light sound interaction length, subject to the limitation that the interaction length is small

$$\frac{k^2 l}{nk} \ll 1, \quad (\text{B3})$$

where k is the acoustic wave number, $2\pi/\lambda$, and k is the optical wave number, $2\pi/\Lambda$.

In the original Raman-Nath formulation, l is simply the depth of the sound beam. The acoustic pressure amplitude along the light path is assumed to be a step function, different from zero only over the interval of depth l and of constant amplitude in this interval. For the more realistic case of a sound beam, which varies in intensity along the light path, the product lP should be replaced by the integral $\int P(x) dx$ for light propagating in the x -direction. A new light-sound interaction distance l^* can then be defined as

$$l^* = \frac{1}{P_m} \int_{-\infty}^{+\infty} P(x) dx, \quad (\text{B4})$$

where P_m is the maximum pressure amplitude. This was shown to be valid in a rigorous treatment by Leroy and Claeys (1984) for the case of a sound beam of Gaussian profile.

They found $l^* = \pi^{\frac{1}{2}} W$, W being the width of the peak at which the pressure equals $1/e P_m$. Note that the integral $P(x)dx$ is proportional to the change in optical path length caused by the presence of the sound field.

Diffraction of light from the focal zone

Near the focus of a converging acoustic wave, the initially spherical wave front gradually flattens out and can be represented approximately as having plane wave fronts (Fig. 17). This can be understood from the simple argument that at the focus the wave must gradually undergo a shift from spherically converging to spherically diverging. This property can be utilized to calculate the diffraction of light from the focal region.

The focused sound wave has approximately planar wave fronts, however, it does not have a uniform pressure amplitude. Rather, its radial pressure distribution in the focal plane is described by the Debye solution in elementary diffraction theory

$$P(r,t) = P_f e^{i\omega t} \int_0^{\alpha_m} J_0(kr \sin\alpha) \sin\alpha \, d\alpha, \quad (B5)$$

where P_f is the peak pressure amplitude in the focal plane, α_m is the half aperture angle of the radiator, ω is the frequency of the sound wave, and J_0 is the zeroth order Bessel function.

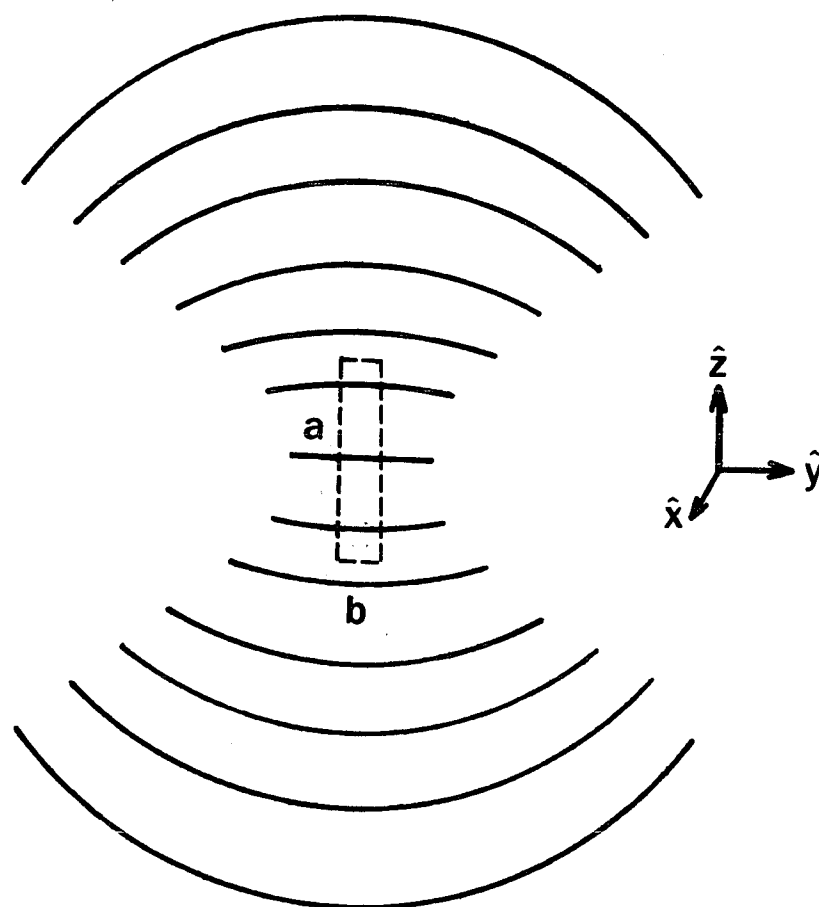


Figure 17. In the parafoveal region of a focused sound beam, the initially spherical wave front flattens out and can be approximated by plane wavefronts traveling in the z direction. The dashed box represents the shape of the light beam incident from the x direction. The beam should be several acoustic wavelengths broad in the z direction in order to produce a clear diffraction pattern, but very narrow in the y direction to sample only the axial portion of the sound field.

For $\alpha_m \leq \pi/6$, $\sin \alpha \approx \alpha$ and the time independent pressure distribution (Fig. 18) can be approximated as

$$P(r) = P_f \frac{2J_1(kr\alpha_m)}{kr\alpha_m} \quad (B6)$$

If $\alpha_m > \pi/6$, then the integral can be solved by series expansion. The special case of $\alpha_m = \pi/2$ is of considerable practical importance and is easily written as a recursion relation

$$P(r) = P_f \sum_{j=0}^{\infty} A_j \quad (B7a)$$

$$A_0 = 1 \quad (B7b)$$

$$A_j = - \left[\frac{kr}{2} \right]^2 \frac{2}{j(2j+1)} A_{j-1} \quad (B7c)$$

The zeroes of this function occur when $kr = m\pi$ where $m = 1, 2, 3, \dots$

With the approximation that the sound waves near the focus of the transducer are quasiplane waves having a pressure profile $P(r)$ along the light path, an effective diffraction length can be calculated for a light beam which is narrow compared to the central maximum of the acoustic focal zone

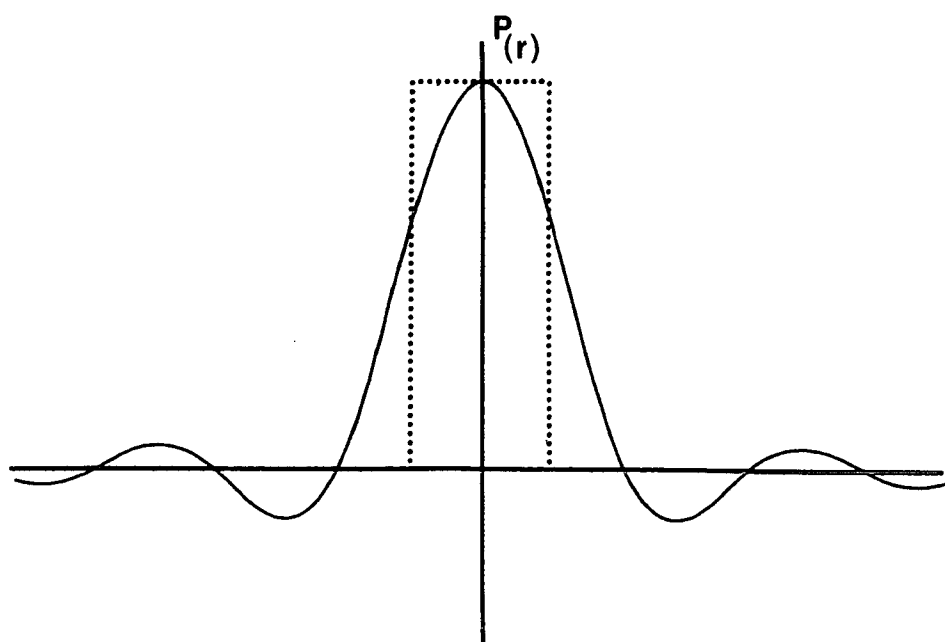


Figure 18. The radial pressure distribution in the focal plane of the transducer (solid line) is replaced by a pressure distribution with a constant pressure amplitude equal to the peak focal pressure and extending over a distance l . The areas under the two curves are the same.

$$1^* = \frac{2}{P_f} \int_0^R P(r) dr . \quad (\text{B8})$$

In the special case of $\alpha_m = \pi/2$ the result of integration is

$$1^* = 2R \sum_{j=0}^{\infty} B_j \quad (\text{B9a})$$

$$B_0 = 1 \quad (\text{B9b})$$

$$B_j = - \frac{2(2j - 1)}{j (2j + 1)^2} \left[\frac{kR}{2} \right]^2 B_{j-1} . \quad (\text{B9c})$$

In the limit as R goes to infinity, 1^* approaches $\lambda/2$ where λ is the acoustic wavelength. The result is shown in Fig. 18 by the dotted line.

Diffraction from a focused shock wave

The results of the last section, for sinusoidal waves can be extended to an arbitrary continuous wave if the Fourier series expansion converges rapidly. The condition of rapid convergence of the series is necessary to insure that the curvature of the phase fronts for the higher harmonics do not invalidate the approximation of plane fronts in the parafocal region. Each harmonic in the series contributes a pressure distribution in the focal plane given by Eq. B5 provided the substitutions $P_f \rightarrow a_j P_1$

$\omega \rightarrow j\omega$, $k \rightarrow jk$ are made. Here a_j is the ratio of amplitudes of the j th harmonic to the fundamental multiplied by a phase factor, and P_1 is the pressure amplitude of the fundamental at the focus. The radial pressure distribution is given by the linear superposition of the harmonic distributions

$$P(r,t) = P_1 \sum_{j=1}^{\infty} a_j e^{ij\omega t} \int_0^{\alpha} J_0(jkrsin\alpha) \sin\alpha \, d\alpha. \quad (B10)$$

For the purpose of Raman-Nath calculations Eq. B10 should be evaluated at a time, t' , such that the pressure at the focus, P_f , is a maximum. With this understanding Eq. B8 can be directly applied to $P(r,t')$ to obtain l^* . However, Eq. B1 is no longer valid. The modifications necessary will be discussed in the next section.

The most important example where the harmonic analysis is useful is in the case of a shock wave in a dissipative linear medium. The shock wave does not attain a true sawtooth waveform because the higher harmonics are strongly absorbed, therefore the Fourier series rapidly converges and the approximation of flat wave fronts does not lead to serious error. In order to visualize the effect of the higher harmonics it is necessary to note that for shock waves the phase relations between the a_j coefficients are such that $P_f > P_1$. The distribution

$P(r,t')$ is therefore more peaked than the distribution for the fundamental, which implies that l^* is narrower.

APPARATUS AND PROCEDURE

A focusing piezoelectric transducer of Channel 5400 Navy I ceramic was held in a dewar with transverse optical windows. Supported at two points by TeflonTM and at a third point by a gold electrical contact, the transducer was operated at its series resonance of 566 kHz while immersed in superfluid helium at 1.9 K. The inner radius measured 0.625 cm and the aperture angle was $\pi/2$. It was necessary to cut two notches in the rim of the transducer for optical access to the acoustic focal zone, half of which lies below the rim (Fig 19).

The light source was a helium-neon laser which had a beam diameter, a , of 0.8 mm at half maximum, just broad enough to illuminate two wavelengths of the sound field, but too wide to resolve the central pressure maximum. In order to sample the peak acoustic pressure in the focal plane of the ultrasound, a +7.5 diopter cylindrical lens was inserted in the optical path. This focused the light to a beam width, b , of 0.07 mm in a direction perpendicular to the propagation of the ultrasound (Fig. 17). Since the resulting beam was narrow (0.2 acoustic wavelengths) compared to the central pressure maximum (one acoustic wavelength) the light only sampled the peak

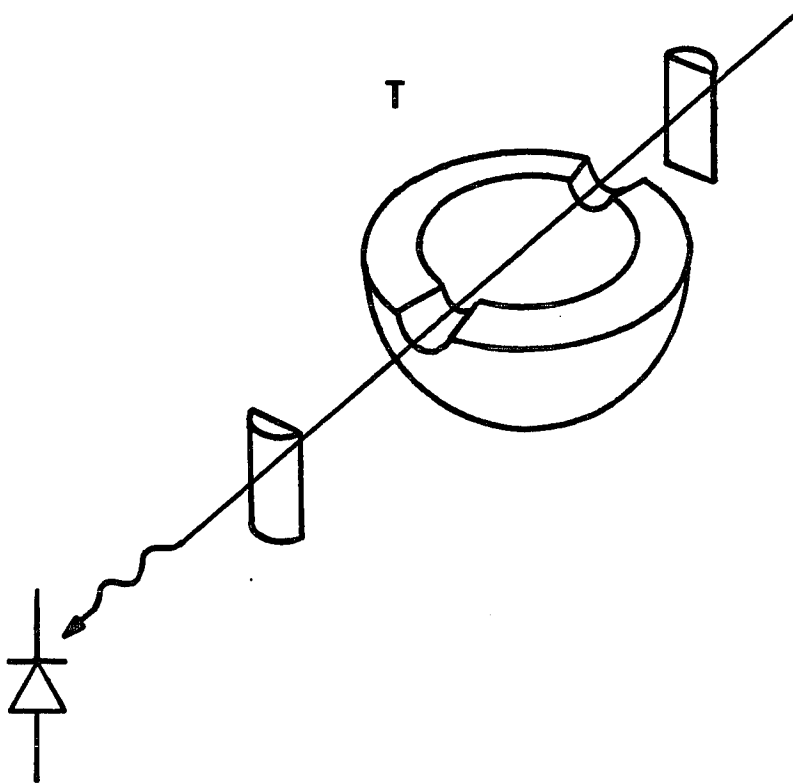


Figure 19. Laser light is shaped by a cylindrical lens and brought to a focus coinciding with the acoustic focal zone of a piezoelectric transducer, T. Access to the acoustic focal zone is obtained through two notches cut along the rim of the transducer which, except for the notches, is a hemispherical shell. After being recollimated by a second cylindrical lens, the zero order diffraction intensity is measured by a photodiode.

pressure amplitude, p_f . After passing through the sound field the laser beam was recollimated with a +2.5 diopter cylindrical lens. The intensity of the central light diffraction order was monitored with a UDT 455 photodiode placed 1.5 meters from the ultrasonic transducer to insure distinct separation of diffraction orders and Fraunhofer conditions. The central diffraction order was chosen because it is relatively immune to finite amplitude effects, such as the formation of higher harmonics which will be discussed in the next section.

Figure 20 shows a typical oscilloscope trace of the output of the photodiode. During the first 0.3 ms after the power to the ultrasonic transducer was turned on, the acoustic pressure amplitude builds to its steady-state value causing the undiffracted light intensity to decrease. After steady state is reached, the intensity of the zeroth order is proportional to the height I_0 and the total diffracted light is proportional to the height ΔI . Taking advantage of the recursion relation for Bessel functions

$$2nJ_n(v) = v(J_{n-1} + J_{n+1}), \quad (\text{B11})$$

and noting that for an acoustic sine wave the intensity of the diffraction pattern is symmetric around the central diffraction order, the ratio $\Delta I/I_0$ can be calculated as a

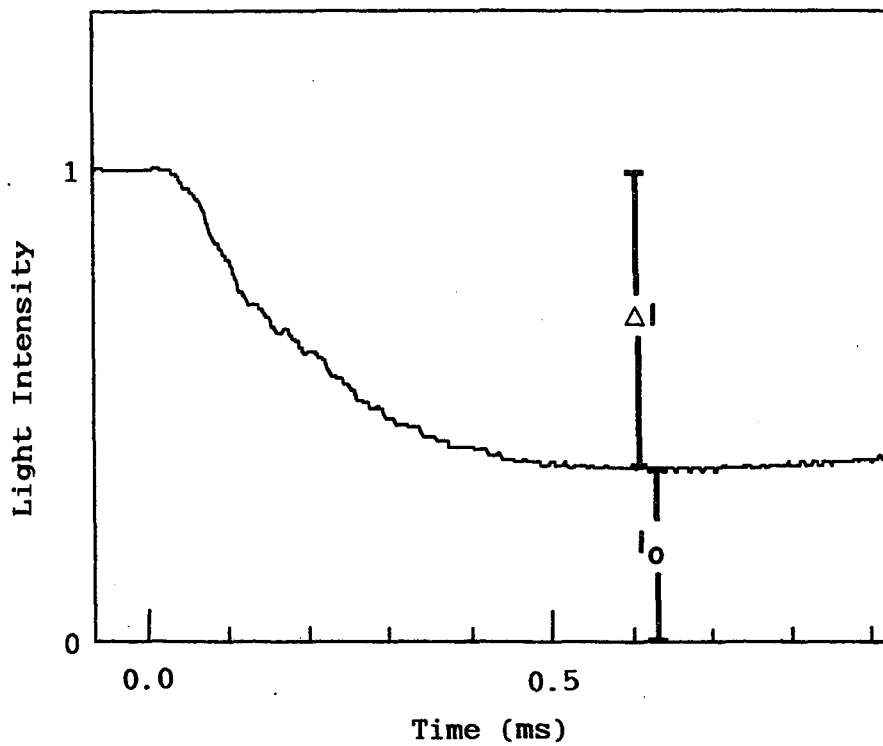


Figure 20. The zero order diffracted light intensity in the first 0.8 ms after power is applied to the piezoelectric transducer. The transducer is operated at its resonance frequency and takes 0.3 ms to build to its full displacement amplitude. When steady state is reached, the intensity of the zero order, I_0 , and the total intensity diffracted into the higher orders, ΔI , are measured.

function of v to any degree of accuracy desired

$$\frac{\Delta I}{I_0} = \frac{2}{J_0^2(v)} \sum_{n=1}^{\infty} J_n^2(v) . \quad (\text{B13})$$

The measurement of the Raman-Nath parameter by the method described above assumes sinusoidal waves and needs to be modified for shock waves. Zankel and Hiedemann (1961) found that the amplitude $\phi_n(v)$ of the n th diffraction order can be calculated by considering the Fourier components of the acoustic wave

$$2 \frac{d\phi_n}{dv} - \sum_j a_j (\phi_{n-j} - \phi_{n+j}) = 0. \quad (\text{B14})$$

Here again a_j is the ratio of the pressure of the j th harmonic of the acoustic wave to the fundamental times a phase factor of +1 or -1, and v is the Raman-Nath parameter for the fundamental. The solutions of Eq. B14, for the case of a pure sine wave, are the Bessel functions of Eq. B1. For a shock wave Eq. B14 leads to an asymmetry in the diffracted light pattern but does not greatly affect the total diffracted intensity. The experimental measurement $\Delta I/I_0$ therefore is essentially a measurement of the fundamental pressure amplitude. As an example, consider the measurement of $\Delta I/I_0$ for a distorted sine

wave with a second harmonic one fourth the amplitude of the fundamental. The value of the Raman-Nath parameter obtained from Eq. B13, which assumes only the presence of the fundamental, is at most 2 percent greater than the value obtained from the more exact calculation utilizing Eq. B14. On the other hand the peak pressure for the distorted wave is 10 percent greater than the fundamental amplitude.

RESULTS AND DISCUSSION

Figure 21 presents the experimentally obtained Raman-Nath parameter for the fundamental frequency vs. the peak acoustic pressure (see the appendix for the calculation of pressure amplitude at the focus). The theoretical result for $l^* = \lambda/2$ is displayed by the solid line for comparison. The agreement is excellent for pressure amplitudes less than the threshold for the formation of shock waves at approximately 3.7 bars. The dashed line is the theoretical result for a distorted sine wave with a second harmonic equal to one fourth the amplitude of the fundamental. Finally the case of a shock wave is represented by the dotted line where the second harmonic amplitude is equal to one half the fundamental. As the second harmonic grows the Raman-Nath parameter continuously moves from the predicted line for the fundamental to the predicted line for the shock wave.

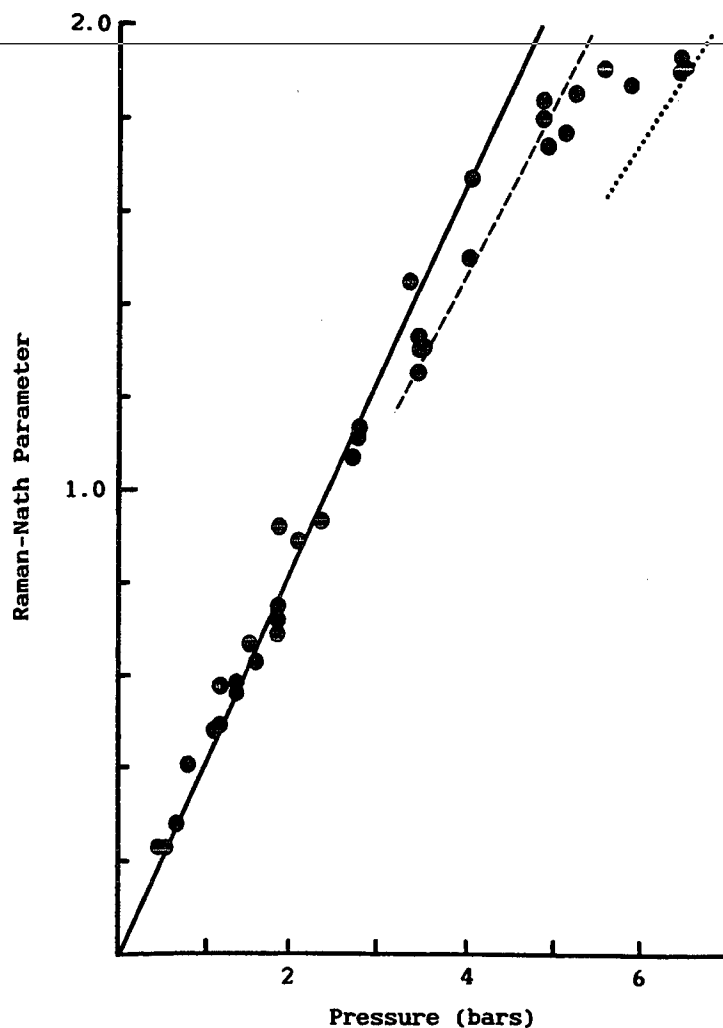


Figure 21. The solid line represents the theoretically obtained Raman-Nath parameter as a function of pressure calculated from Eq.2 with $l = l = \lambda/2$. Also plotted are experimentally obtained values of the Raman-Nath parameter at different pressure amplitudes based on the assumption of there being no second harmonic present in the ultrasound. At pressure amplitudes above 3.7 bars a second harmonic is generated and this assumption breaks down. The experimental values deviate smoothly from the predicted line for a single harmonic, crossing the correction for a sound beam with a second harmonic one fourth the fundamental amplitude (dashed line), and reaching the theoretical result for a second harmonic one half the fundamental amplitude (dotted line).

Although it should be possible, no attempt was made in this study to directly measure the amplitudes of the harmonics of the shock wave. By measuring the asymmetry in the diffracted light pattern, Eq. B14 or its equivalent (Cook 1965) can be used for the harmonic analysis.

CONCLUSION

This paper reports a method to measure the peak acoustic pressure of a spherically focusing transducer utilizing the diffraction of light. Nagai (1986) has shown that due to the curvature of the wavefront, the elementary Raman-Nath treatment of light diffraction leads to large errors when applied to spherically focusing transducers with aperture angles greater than 5° . However, we have shown that by restricting the measurement to the focal zone where the wavefronts are approximately planar, the Raman-Nath approach can be utilized with aperture angles up to 90° . An effective interaction distance can be defined which adequately takes into account the pressure profile of the focal zone.

The motivation for this study was to measure the pressure amplitude in liquid helium tensile strength experiments; however, there are other fields of research where this method would be useful such as focused ultrasound waves for medical diagnostics and treatment, and measurement of the sound field of acoustic

microscopes.